Measurement of the dynamic range of SiPMs for Auger Prime

Bachelorarbeit in Physik

von

Alexander Gutsche

vorgelegt der
Fakultät für Mathemtik, Informatik, Naturwissenschaften
der
Rheinisch-Westfälischen Technischen Hochschule Aachen

im August 2016

Erstgutachter	Zweitgutachter
Prof. Dr. Thomas Bretz	Prof. Dr. Thomas Hebbeker
III. Physikalische Institut A	III. Physikalisches Institut A
RWTH Aachen	RWTH Aachen

Contents

1 Introduction

In this Bachelor thesis the dynamic range measurement of two different Silicon Photomultipliers for the upgrade of the Pierre Auger Observatory, Auger Prime will be presented.

In the first chapter a short introduction to Ultra-High Energy cosmic rays, the actual Pierre Auger Observatory and the upgrade is given.

After an explanation of the functionality of Silicon Photomultipliers, the main characteristics will be presented.

An introduction to the optical test set-up gives the following chapter. This optical test set-up was developed by Carsten Heidemann in his PhD-Thesis at RWTH Aachen University.

At first the determination of the breakdown voltage of the two SiPMs will be presented. The errors of this measurement with a temperature-dependent quenching and protective resistance will be discussed and measured.

The dynamic range measurement is presented in the following chapter with different analysis methods. A measurement of the temperature dependency of the dynamic range is also done in this chapter.

In the last chapter a Monte Carlo simulation for the dynamic range will be envisaged. The results from the measurement will be compared with the results from the simulation. Also an simulation with homogeneous light flux will be done.

2 Ultra-high energy cosmic rays and the Pierre Auger Observatory

This chapter gives a short introduction to Ultra-High Energy Cosmic Rays (UHCERs) and the Pierre Auger Observatory located in Malargue, Argentina. It will also give a short introduction into the upgrade of the Pierre Auger Observatory Auger Prime.

2.1 Ultra-high energy cosmic rays

Cosmic rays were discovered by Victor Hess in a series of balloon flights in 1912. He found that the ionization rate above an altitude of 2500 m was increasing instead of decreasing what was thought at this time. He assumed that cosmic rays to be electromagnetic in nature [1]. For his discovery he was awarded the Nobel prize in physics in 1936 [2].

Today, the composition of cosmic rays is well known. Only the composition of the cosmic rays with ultra-high energy is nearly unclear.

Ultra-High Energy Cosmic Rays are highly energetic particles with a kinetic energy higher than $10^{18}\,eV$. These high energy particles around the Ankle of the Cosmic Ray Spectrum are really rare, with a flux of one particle per square-kilometre and century. These low fluxes make it hard to measure UHECRs because large sensitive areas and a lot of time are needed to measure one particle [3].
The primary particle are not detected directly with a ground detector. By interacting with the air molecules in an altitude of tens of kilometres the primary particles decay and occur secondary particles. These secondaries induce themselves a new cascade, so that a massive growth is initialised and continues as long as the energy of the generated particles are able to compensate the ionisation energy [3, 4]. These air showers travel nearly with the vacuum speed of light towards the ground. Such an extensive air shower is shown schematically in 2.1.

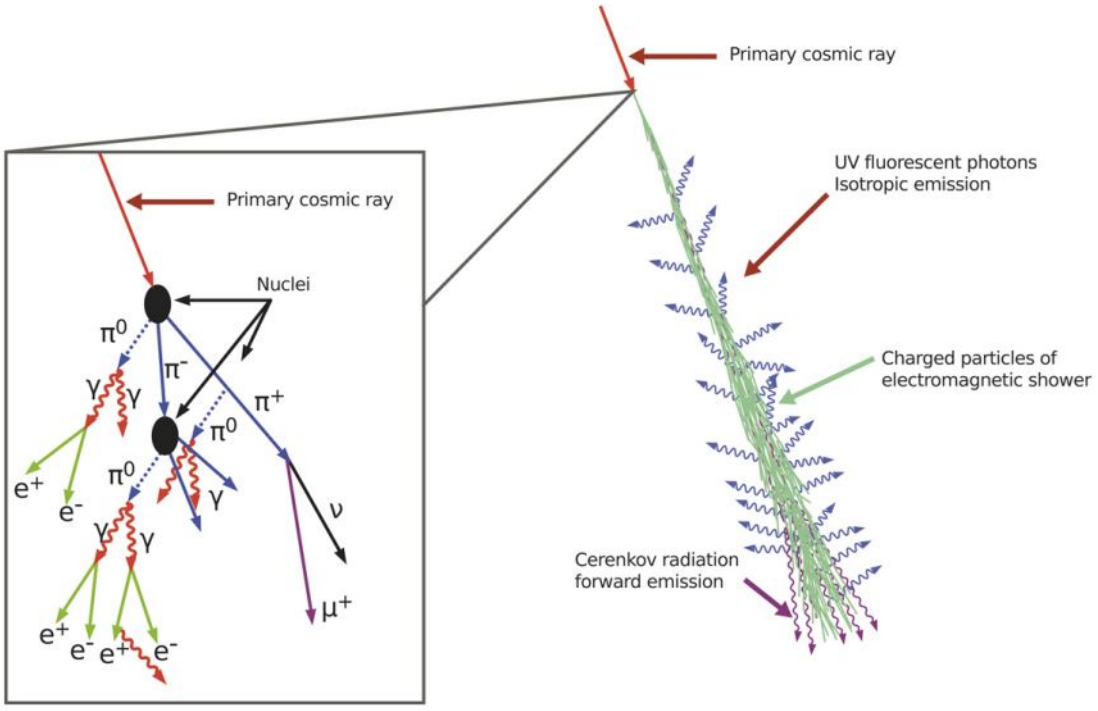

Figure 2.1: Schematically diagram of an extensive air shower [5]

.

2.2 The Pierre Auger Observatory

The Pierre Auger Observatory is located in the western Mendoza Province in Argentina and named after the French physicist Pierre Victor Auger. The Pierre Auger Observatory measures these secondary cosmic ray particles over an area of $3000\,km^2$ with 1660 surface detector stations (SD). The surface detector stations are arranged in a triangular grid with $1500\,m$ distance between them [3, 6, 7].
These surface detectors are water Cherenkov detectors. They are made of tanks filled with twelve tons of ultra pure water. If a secondary particle goes through the water Cherenkov light will be emitted. Three photomultiplier tubes (PMTs) measure the Cherenkov light in every detector station [7].
The Pierre Auger Observatory also hosts 27 fluorescence telescopes located in five buildings measuring the longitudinal shower profile, see Figure 2.1 [6, 7].

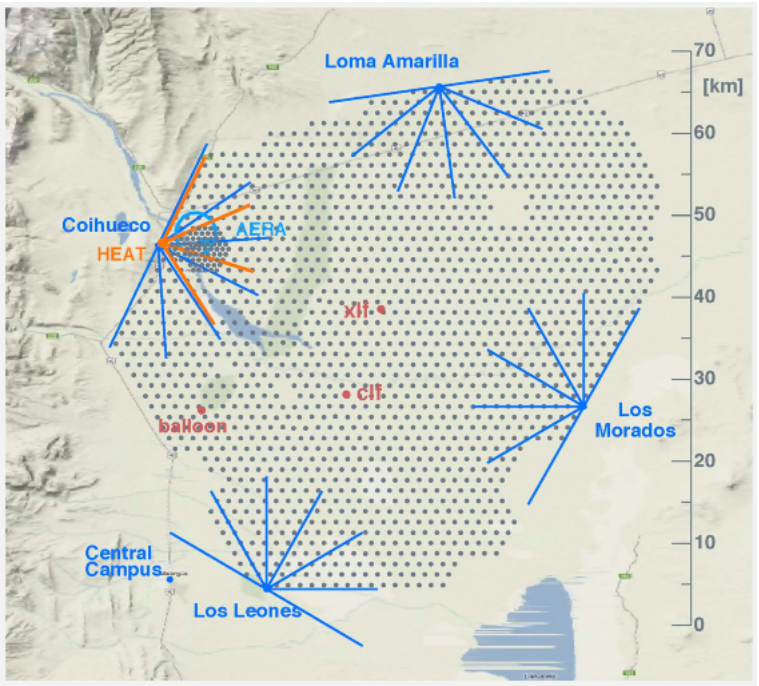

Figure 2.2: Schematical picture of the Pierre Auger Observatory. Every dot represents a water Cherenkov detector [8].

2.2.1 Auger Prime

Auger Prime is the name of the upgrade of the Pierre Auger Observatory. This chapter just gives a short introduction to one part of the upgrade, the Surface Scintillator Detector (SSD).
The Surface Scintillator Detector consist of two $2\,m^2$ extruded plastic scintillator modules which are coupled with wavelength-shifting (WLS) fibres to a photon detection device [9].
In a first design presented in the Auger Prime design report every scintillator plane is made of twelve scintillator bars. Each of these bars is $1.6\,m$ long, $10\,cm$ wide and $1\,cm$ thick. Four WLS are embedded in each of these bars. The bars of one module are glued to an extruded polystyrene plane, forming a grid structure [9].
A schematic view of the two modules with the scintillator bars is shown in Figure 2.3. The light from all the WLS will be detected with a photon detection device. This device is mounted between the two planes in an extra chamber with a mobile door. This door gives an access to the photon detection device.
The external box of the detector is made from aluminium to guarantee light tightness and robustness for 10 years operation in the field [9].
This Box with the two planes is enclosed by a double aluminium roof, separated by

2 *cm*. These separation allows air flow and reduce the temperature changes [9].
The scintillator will be mounted on the top of the water-Cherenkov detector, shown in Figure 2.4.
It is possible to mount a photomultiplier tube (PMT) or two Silicon Photomultipliers (SiPMs) at the place of the photon detection device. SiPMs have some advantages compared to normal PMTs. The SiPM is much smaller than a normal PMT and it is possible to measure single photon events in case of the high amplification of the Geiger mode.

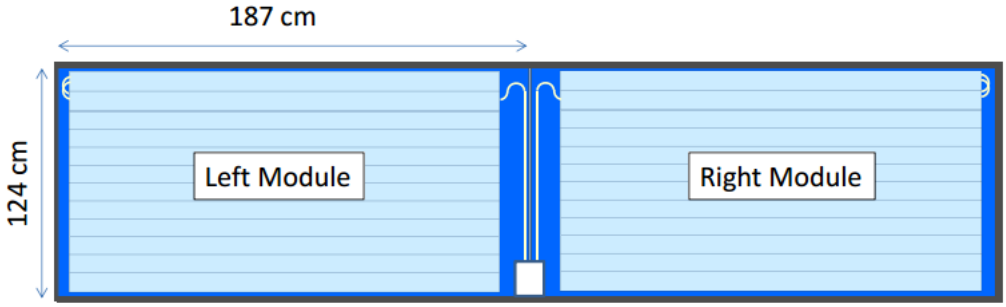

Figure 2.3: Schematica view of the SSD scintillator bars [9].

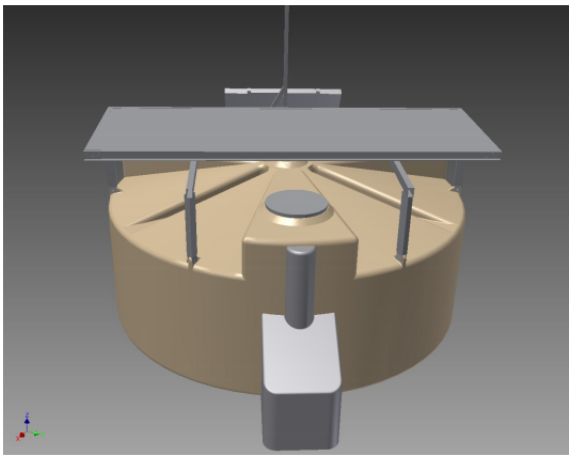

Figure 2.4: Water-Cherenkov detector with surface scintillator detector [9].

3 SiPM introduction

This chapter will give a short introduction to Silicon Photomultipliers.
Silicon Photomultipliers (SiPMs) are solid-state based Geiger avalanche photo detectors, that can produce a current pulse in response of absorption of a photon tens of nanoseconds long.

3.1 SiPM structure

SiPMs are pixelated devices with up to $56,700$ cells for the $6 \times 6\,mm^2$ SiPM that are studied in this thesis. Each of these cells is a series combination of an avalanche photodiode (APD) and a quenching resistor (QR). All the micro-cells are connected in parallel. The circuit diagram is shown in Figure 3.1.
There are Silicon Photomultipliers with different cell pitches and sizes.
Each cell of an SiPM outputs a pulse at the same size when it detects a photon. These pulses are superimposed onto each other, so the height of the output pulse can be measured [10].

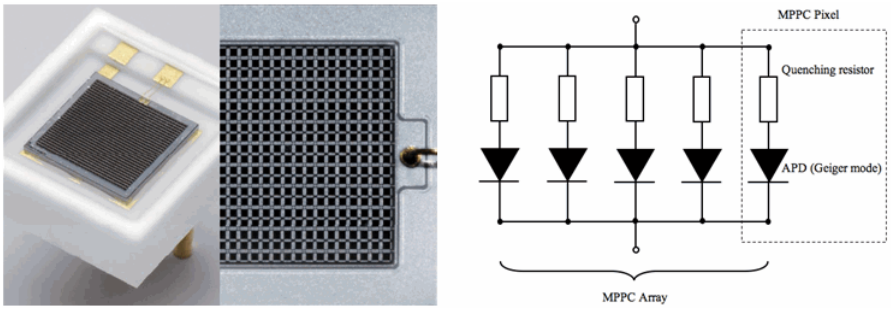

Figure 3.1: Structure of a silicon photo multiplier and equivalent circuit [10].

The discharge and the recharge of a cell of the SiPM appears as a current pulse. The discharge phase corresponds to the rising edge of the pulse, while the falling edge corresponds to the recovery phase, shown in Figure 3.2. The time constant of the falling edge can be calculated with the diode capacitance and the quenching resistance to: $\tau_{recovery} = Cd \times Rq$ [11]. The recovery of cell can be approximated by an exponential function: $\approx exp\left(\frac{-t}{R_Q \times C_d}\right)$. A schematic pulse is shown in Figure 3.2. The total recovery time from the SiPMs is $20\,ns$ for the SiPM with a $25\,\mu m$ cell pitch and $50\,ns$ for the

SiPM with the 50 μm cell pitch [12]. With the total recovery time the time until the SiPM is total recharged and can produce an pulse with the maximum height.

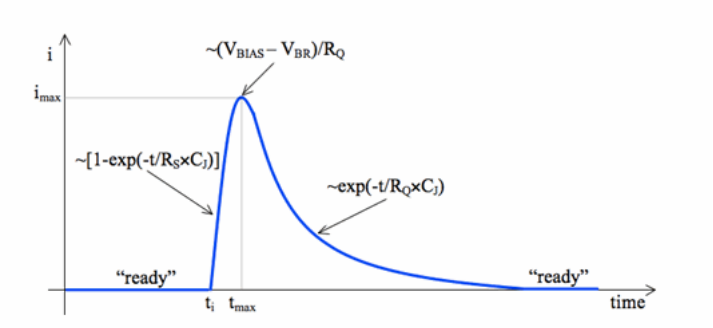

Figure 3.2: Pulse of a fired SiPM cell with the rising and the falling edge [10].

3.2 Bias, breakdown and overvoltage

In a normal application, an external source V_{bias} is applied on the SiPM so that every cell can operate in Geiger mode. The bias voltage has to be larger than the breakdown voltage of the SiPM because this is the minimum voltage that leads to self sustaining avalanche multiplication in Geiger-mode avalanche photo diodes. The breakdown voltage depends on different characteristics of the SiPM [11, 13].
The overvoltage is known as the difference between the bias and breakdown voltage.

$$V_{ov} = V_{bias} - V_{breakdown}$$

The overvoltage is an important parameter affecting the operation of a SiPM. The higher the overvoltage the higher the SiPM performance. A higher overvoltage caused an higher noise.
A significant characteristic of the breakdown voltage is its temperature dependency. The breakdown voltage goes linear with the temperature change. It is possible to calculate the breakdown voltage with the following linear equation:

$$V_{br}(T) = V_{br}(0\,°C) + \beta(T - 0\,°C) \tag{3.1}$$

$V_{br}(0\,°C)$ equals the breakdown voltage at $0\,°C$ and β is the temperature dependency of the breakdown voltage. It is important to know the breakdown voltage of an SiPM exactly for using it as a photon detection device.
The charge Q of the avalanche of one pixel can be calculated with:

$$Q = C \cdot V_{ov} = G \cdot e,$$

with C the capacitance of one micro cell, e the elementary charge and G the gain of the SiPM.
It is not easy to measure the exact breakdown voltage because there are several different methods that show small variations in their expected results [11, 13, 14].

3.3 Photon detection efficency

The photon detection efficiency (PDE) is the probability that a photon can fire a cell of a SiPM. It depends on the overvoltage V_{ov} and the wavelength λ of the incident light. The PDE can be expressed as a product of three different parameters. f the geometrical fill factor, $\eta(\lambda)$ the quantum efficiency and ϵ_V which is the probability of Geiger discharge.

$$PDE(V_{ov}, \lambda) = f \cdot \eta(\lambda) \cdot \epsilon(V_{ov}) \tag{3.2}$$

The geometrical fill factor f comes from the circumstance that the SiPM has a cell structure. Between these pixels are areas that have no photosensitivity. In this areas are connections between the cells and quenching resistors. The fraction of the photosensitive area and the total area is known as the geometrical fill factor. The value of the geometrical factor depends on the cell pitch or to be precise the area of each cell of the SiPM A_{cell} and the distance between two cells and N is the number of cells on the SiPM.The quantum efficiency η is the probability that a photon can produce a electron hole pair [11, 13, 15].

$$f = \frac{A_{cell}}{(\sqrt{A_{cell}} + \frac{N-1}{N} \cdot d)^2}$$

The geomterical fill factor ranges between $\sim 30\%$ and $\sim 80\%$.
The quantum efficiency η is the probability that a photon can produce a electron hole pair [15].

3.4 Gain

The gain of a SiPM is the number of charge carriers that are contained in a single-cell current pulse. Without any excess noise this single pixel discharge is equivalent to the gain of the SiPM. Therefore in a first approximation the gain of a SiPM is scaling linear with the applied overvoltage. The calculation could be done with the same formula like in the section about the overvoltage.

$$G = \frac{V_{ov} \cdot C_{micro-cells}}{e}$$

$C_{micro-cells}$ is the capacitance of one micro-cell. With a known gain G it is possible to calculate the charge flow that occurs when one cell is hit by a photon [10].

3.5 Noise

The noise of a SiPM limits the smallest signal that can be measured. There are different types of noise, primary and correlated noise.

Dark count rate

The main source of noise is the dark count rate. There is a finite probability for carriers to be generated by thermal agitation. During the quiescent mode, if an electron or a hole originates inside the active region of a G-APD an avalanche is initiated and an output pulse can be observed. The number of dark events per unit time is called the dark count rate. The dark count rate is a function of temperature, overvoltage, detection area and micro-cell size. The thermal generation of carries doubles approximately every 10 K [11].

Optical crosstalk

Optical crosstalk is a special component of SiPM noise. It is correlated noise and originates from an existing pulse. The optical crosstalk happens nearly simultaneous with the absorbation of the main photon or a noise photon.
Optical crosstalk appears if a cell is fired by a photon or by thermal noise.
The schematic mechanism of direct/prompt, delayed and no crosstalk is shown in 3.3.

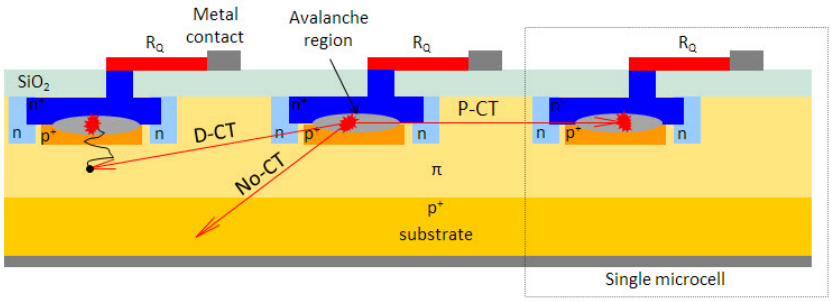

Figure 3.3: Schematic mechanism of prompt (P-CT), delayed (D-CT) and no (NO-CT) crosstalk with three representative photons [16].

The optical crosstalk depends on different characteristics of an SiPM: the size of an micro-cell, the layered architecture and the overvoltage. The first two parameters

are fixed for a given SiPM but the probability increases with increasing overvoltage [16]. Optical Crosstalk is a really small effect. In the studied SiPM it happens with a probability between 1 % and 3 % if a cell is fired [17].

Afterpulsing

Afterpulsing events are like crosstalk events originated from an existing current pulse. For this reason afterpulsing is also referred to correlated noise. Afterpulsing is based on carriers trapped in silicon defects during the avalanche. These carriers are released later on during the recharge phase of the Geiger mode avalanche photo diode. With this effect a new current pulse on the tail of the original current pulse can be observed. The probability of afterpulsing increases more than linearly with the over voltage and quadratically with the cell size as an effect of the increasing gain [11] [10].

3.6 Dynamic Range

The dynamic range of a photodetector can be defined as the optical signal level in which the detector provides a useful output. For a SiPM, this range extends from lowest signal level detectable, to the optical signal level that results in all of the SiPM micro-cells detecting photons simultaneously [18].
The dynamic range is a function of the total number of micro-cells and the PDE of the SiPM. As a function of the PDE it is also a function of the wavelength and the bias voltage. It is possible to approximate the number of fired cells by the following equation

$$N_f(M, V, \lambda) = M \left(1 - exp \left(-\frac{PDE(V, \lambda) \cdot N_\gamma}{M} \right) \right) .$$

N_f represents the number of fired cells, PDE the photon detection efficiency. The PDE depends on the wavelength of the incoming light λ and the overvoltage V_{ov} of the SiPM. M is the number of cells of the SiPM. The number of incident photons where the SiPM is saturated can be calculated by:

$$N_\gamma = \frac{5 \times N_{cells}}{PDE}(1 - p_{crosstalk})$$

with $p_{crosstalk}$ as the probability of a crosstalk event [19].

3.7 Characterised SiPMs

In the following table are the characteristics at 25 °C given by the manufacturer from the two different SiPMs from Hamamatsu, which are studied in this thesis.

SiPM	S13360-6025PE	S13360-6050PE
Pitch size / μm	25	50
Effective photosensitive area / mm^2	6×6	6×6
Number of cells	56,700	14,400
Fill factor / %	47	74
V_{ov} / V	5	3
Photon detection efficiency / %	25	40
Gain	7.0×10^5	1.7×10^6
Crosstalk probability / %	1	3
Spectral response range λ / nm	320 - 900	320 - 900
Peak sensitivity wavelength λ_p / nm	450	450

Table 1: Characteristics stated by Hamamatsu for the studied SiPM [17].

In the following chapters of this thesis the two different SiPMs are distinguished by their pitch size 25 μm and 50 μm.

4 The optical test set-up

The following chapter gives an introduction to the optical set-up for automatised SiPM characterisation. This set-up was developed by Carsten Heidemann at RWTH Aachen University in his PhD-thesis. The set-up inlcudes a light source with LEDs with different wavelength, a temperature stabilization and measurement instruments. Carsten Heidemann also developed a control and data acquisition software, which will also be described in this chapter [20].
A scheme of the optical test set-up is shown in 4.1.

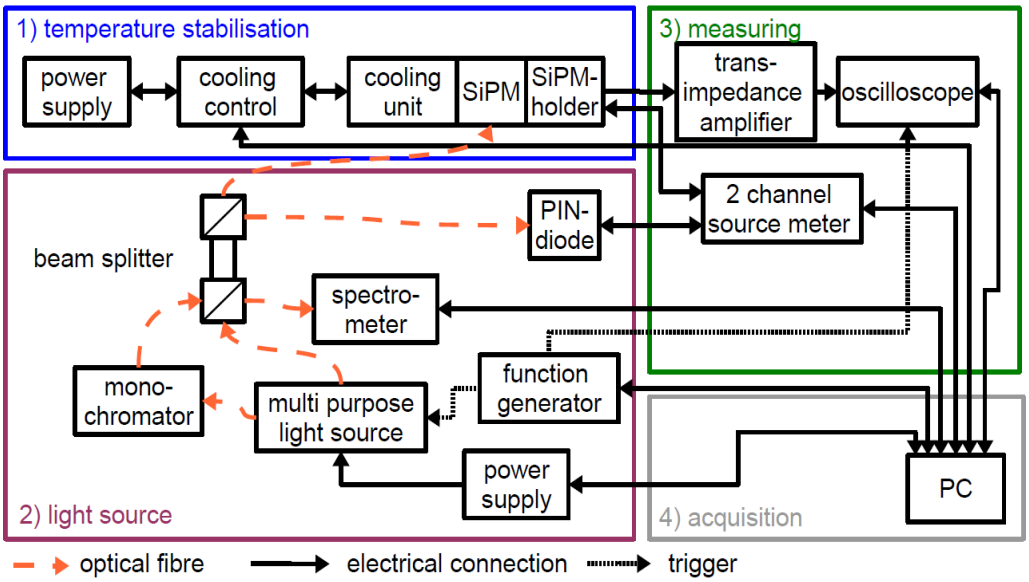

Figure 4.1: Scheme of the optical test set-up with the four main functional groups: the temperature stabilisation, the light source and light distribution, measuring instruments and the data acquisition [20].

4.1 Hardware components

4.1.1 Light source

The light source is a custom-made LED based light source with up to 32 LED modules shown in Figure 4.2. There are two different types of LED modules: a pulser and a

DC (direct current) module.

The DC module offers a stable, continous light flux, while the pulser module offers high voltage pulses with up to $130\,V$ for only a few nanoseconds.
The LED modules are placed in a line so that the fibre header can be moved with a stepper motor between the LED modules. The two fibres on the header allow to couple the light in two different ways into the SiPM. The one fibre goes directly into the beam splitter the other first into a monochromator.

The light spectrum of the different LED modules is shown in Figure 4.3.

For the measurements LED 9 and 10 are used, because they have a wavelength near to the PDE maximum of the tested SiPMs: $\lambda_9 \approx 460\,nm$ and $\lambda_{10} \approx 460\,nm$ [20].
LED 9 have a wavelength range from $\sim 435\,nm$ up to $\sim 500\,nm$ and LED 10 between $\sim 440\,nm$ and $\sim 505\,nm$, see Figure 4.3.

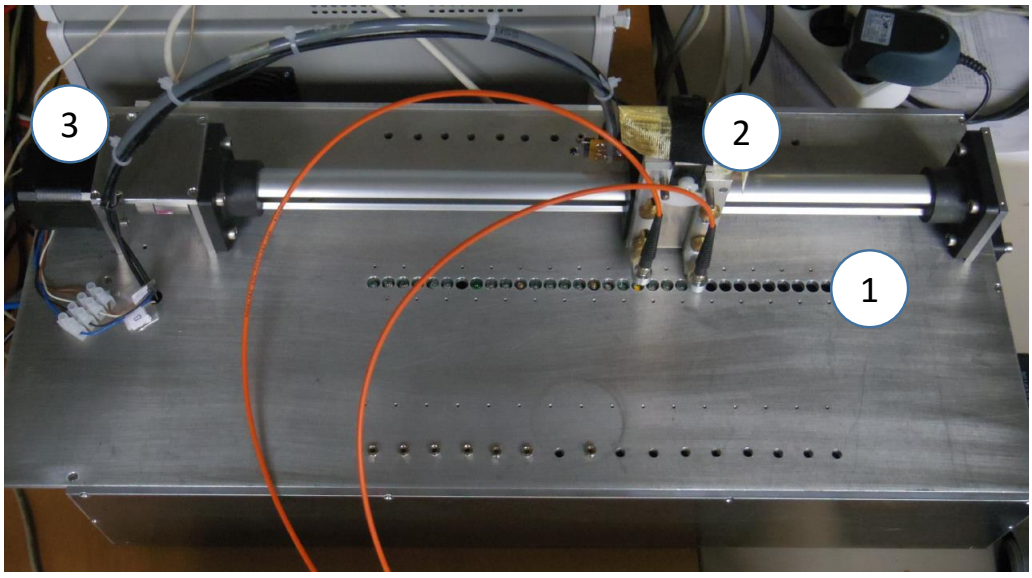

Figure 4.2: Custom-made LED light source with two fibres on the fibre header. Visible the line with the LEDs (1), the movable header with the two fibres (2) and the stepper motor (3) [20].

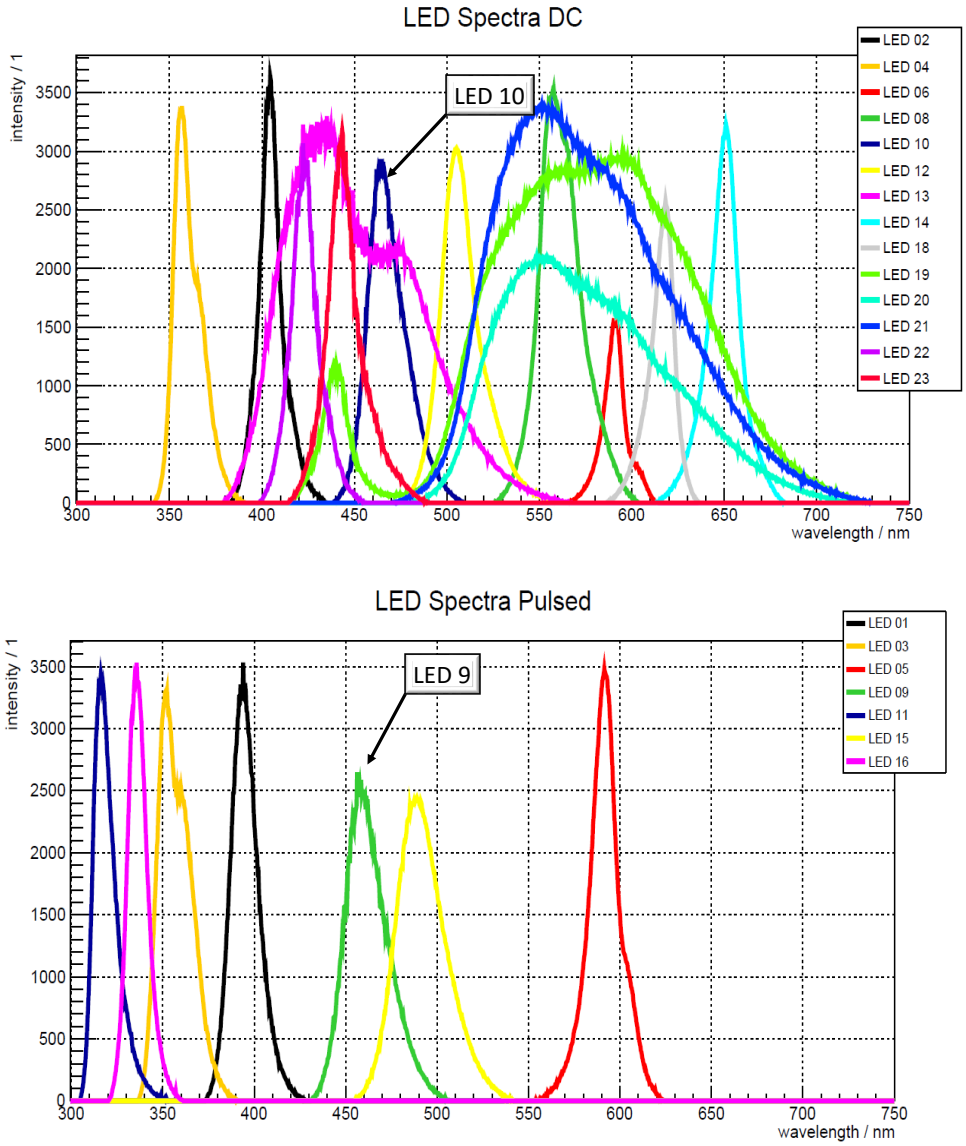

Figure 4.3: LED Light spectra from custom-made LED light source with references to the two used LEDs. In the upper half of the figure the spectra of the DC LEDs and in the lower part the spectra of the pulsed LEDs [20].

4.1.2 Monochromator

The monochromator returns just a small wavelength range of the initial LED wavelength range. A blazed grating expands the incoming light beam to a beam with 1 cm diameter [20]. From this expanded beam a small wavelength range is captured with a moveable fibre.

4.1.3 Beam splitter/Light distribution system

The beam splitter combines the two different fibres from the light source, one direct from the light source, the other from the monochromator. It is built up with two beam splitter, because after the combination of the two beams, the beam will be splitted again into three beams. The partial beam that gets out the first beam splitter is fed into a spectrometer to measure the spectral range of the light beam.

One of the partial beams from the second beam splitter is fed into the reference detector and the other is fed into the SiPM [20].

The output ratio between the two outputs of the second beam splitter was measured by Carsten Heidemann to calculate the exact flux on the SiPM with the informations of the PiN photodiode.

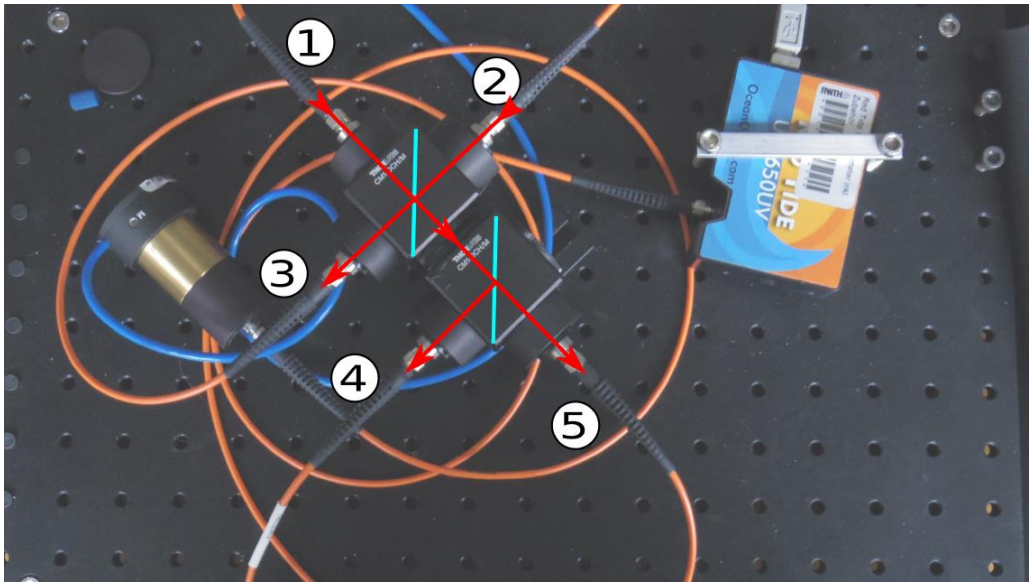

Figure 4.4: Beam splitter of the optical test set-up with the input fibre from the monochromator (1) and direct from the light source (2). The outlet from the first beam splitter into the spectrometer (3). The outlets from the second beam splitter are fed into fibres to the reference PiN diode (5) and the SiPM (4) [20].

4.1.4 Temperature stabilisation and measurement

A stable temperature is important for exact measurements. The temperature stabilisation system of the test set-up is built out of three Peltier elements with an airflow on the hot side of the largest Peltier element [20].

With the control system of the Peltier elements it is possible to heat and cool the copper mass where the SiPM is mounted in. The temperature sensor is also mounted on the copper mass. This set-up offers a stable temperature to the last significant bit of the installed digital temperature sensor with the PID controller ($\Delta T_{stable} \leq 0.07\,K$) [20].

4.1.5 SiPM mount and circuit board design

The optical test set-up is developed for SiPM with pins. In this thesis two surface mounted (SMD) SiPM from Hamamatsu will be characterized. To place them into the optical test set-up a small circuit board was developed, shown in Figure 4.5.

One important thing by using this circuit board is, that the distance between the sensitive surface of the SiPM and the light output of the optical fibre changes and the geometrical factor changes which is used to calculate the photon flux on the SiPM from the flux on the PiN diode. The calculation of the new geometrical factor will be done later in this chapter.

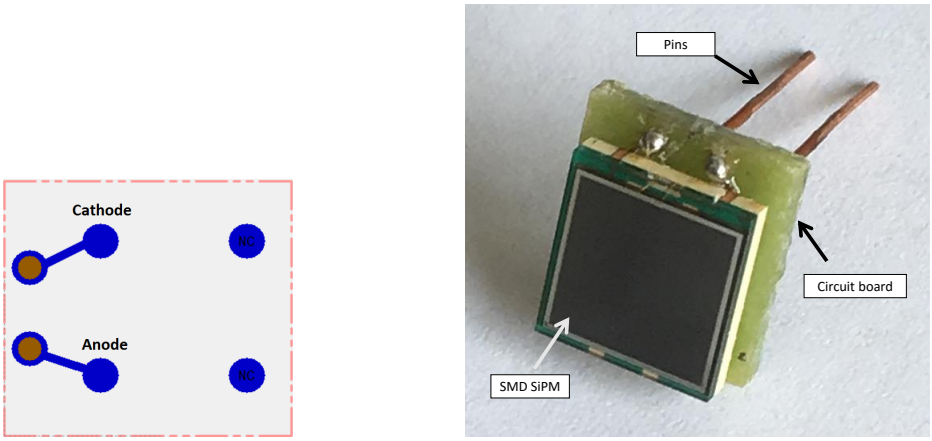

Figure 4.5: Circuit board for a SMD SiPM to mount it in the optical test set-up and one SMD SiPM on the developed circuit board with pins.

With two springs the SiPM is held in place and it also allows a quick change of the SiPM [20]. It is easy to reposition the SiPM at the exact same place what is important for the calibration of the PIN photo diode which is used as reference.

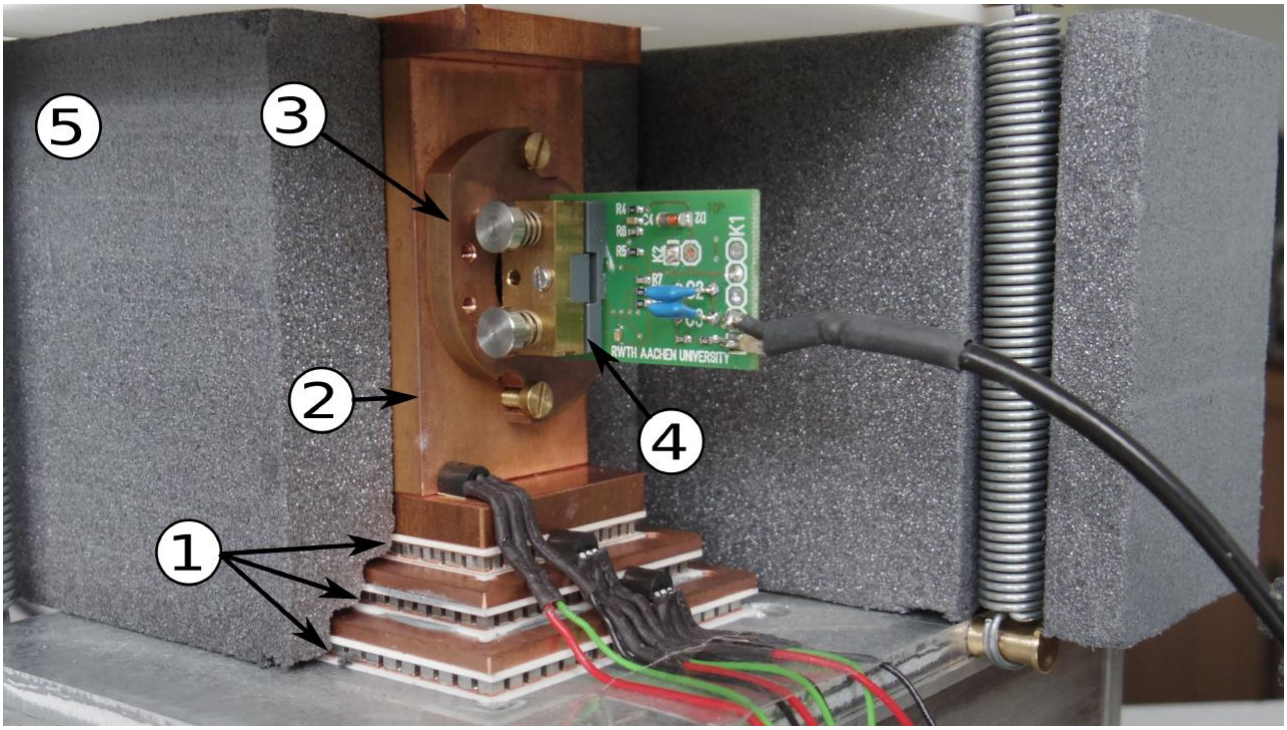

Figure 4.6: The cold copper mass (2) on top of the triple-stacked Peltier elements. The SiPM quick mount (3) with the springs for the SiPM mount (4) and the thermal isolation (5) which is completely closed during a measurement [20].

4.2 Measuring instruments

The measuring instruments are important for precise measurement and the digitalisation and acquisition of the data from the SiPM. This chapter gives a short overview of the different measuring instruments in the optical test set-up.

4.2.1 Oscilloscope

In the test set-up the main measuring instrument is an oscilloscope. It is a fast and precise measuring instrument which offers a sampling rate up to 10 GSaps with a memory depth of 40 MSa. The oscilloscope is used to measure single events. This can be done in two different ways. In one way the oscilloscope measures long traces with 100 ps time step. In the other way the oscilloscope measures up to 8192 short traces in a triggered mode [20].

4.2.2 Sourcemeter

The sourcemeter can not be used to measure single events. The sourcemeter is used for measuring the average flux from SiPM and the PIN diode.

While measuring the average flux from the two detectors it is supporting these with their bias voltage. The measurement setting are an integration over one power line cycle and an internal averaging over 50 internal analog-to-digital conversions. Every point is the average of ten such filtered values [20].

From these ten values a mean and a standard deviation are calculated and saved.

4.3 Beam profile on PIN/SiPM and calculation of the flux on the SiPM

For the calculation of the photon flux on SiPM and PIN diode it is important to know that they do not have the same size, geometry and distance from the fibre, how it is shown in 4.7.

The beam profile that comes from the multimode fibres equals a Gaussian profile. It is possible to calculate the total photon flux on the SiPM surface with a given numerical aperture from the fibre (NA), the distances between fibre end and PiN surface d_{pin} and fibre and SiPM surface d_{sipm}, the edge length of the active area from the SiPM a, the PiN active radius R_{pin}, the constant $b = \sqrt{-\ln(0.05)} \approx 1.730$ [20], the ratio $R_{r/t}$ between the reflected and the transmitted port of the beam splitter and the measured photon flux on the PiN diode $\Phi_{pin,t}$ [20].

In this thesis we just calculate it with the circuit board in the modified set-up.

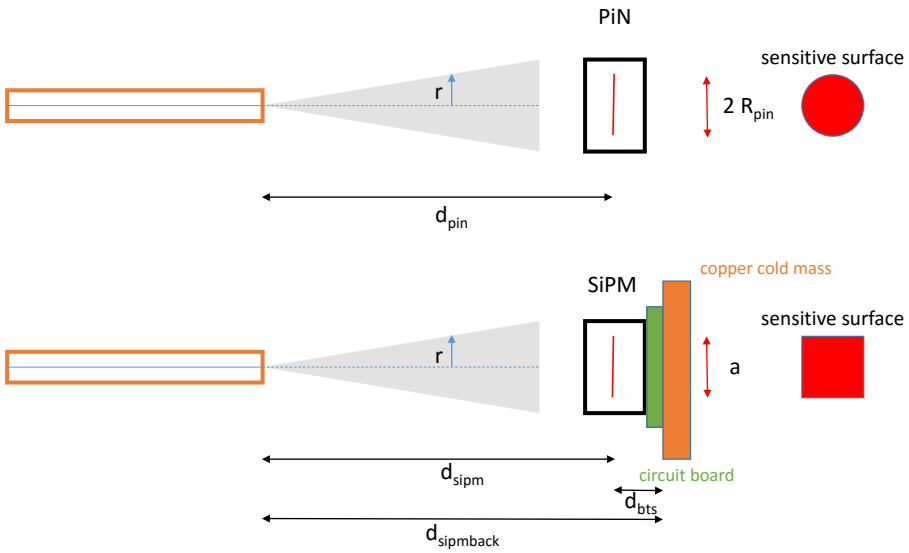

Figure 4.7: Schematic of the distances and parameters used in the beam profile calculation

The beam radius $r_{0.05}$ where the beam intensity has dropped to 5% of its maximum in a distance d from the fibre can be described by:

$$r_{0.05} = \frac{d \cdot \tan(\sin^{-1}(NA))}{b} \tag{4.1}$$

The intensity of the Gaussian beam profile is given by:

$$I(r,d) = I_0(d) \cdot \exp\left(\frac{-r^2}{\sigma^2}\right) \tag{4.2}$$

With the radius $r_{0.05}$ follows:

$$I(r_{0.05,d}) = 0.05 \cdot I_0(d) \tag{4.3}$$

$$\Leftrightarrow \ln(0.05) = \frac{-(r_{0.05})^2}{\sigma^2} \tag{4.4}$$

$$\Leftrightarrow \sigma = \frac{d \cdot \tan(\sin^{-1}(NA))}{b^2} \tag{4.5}$$

The flux on a surface A at a given distance d is given as the integral of the intensity:

$$\Phi_A(d) = \int_A I(r,d)dA = I_0 \cdot \int_A \exp\left(\frac{-r^2}{\sigma^2}\right)\, dA \tag{4.6}$$

For the calculation of the total photon flux, the flux on the SiPM and the flux on the PiN diode three integrals with different integration limits have to be solved.

$$\text{Total photon flux :} \qquad F_{full} = \int_0^{2\pi}\int_0^{\infty} I(r,d)/I_0 \cdot r dr d\phi \tag{4.7}$$

$$\text{PiN photon flux :} \qquad F_{pin} = \int_0^{2\pi}\int_0^{R_{pin}} I(r,d)/I_0 \cdot r dr d\phi \tag{4.8}$$

$$\text{SiPM photon flux :} \qquad F_{sipm} = \int_{-a/2}^{a/2}\int_{-a/2}^{a/2} I(x,y,d)/I_0 dx dy \tag{4.9}$$

The first two integrals are solved by using polar coordinates. The third integral is a little bit more difficult because it has to be solved with the Gauss error function.

$$\text{erf}(x) = \frac{2}{\sqrt{\pi}}\int_0^x \exp\left(-t^2\right)\, dt \tag{4.10}$$

The integrals have the following solutions:

$$\text{Total photon flux} \qquad F_{full} = \frac{\pi \cdot d^2 \cdot NA^2}{b^4 \cdot (1 - NA^2)} \tag{4.11}$$

$$\text{PiN photon flux} \qquad F_{pin} = F_{full} \cdot \left(1 - \exp\left(\frac{b^4 \cdot (NA^2 - 1) \cdot R_{pin}^2}{d^2 \cdot NA^2}\right)\right)^{-1} \tag{4.12}$$

$$\text{SiPM photon flux} \qquad F_{sipm} = F_{full} \cdot erf\left(\frac{\frac{a}{2} \cdot b^2 \cdot \sqrt{1 - NA^2}}{d \cdot NA}\right)^2 \tag{4.13}$$

The light fluxes on the photo diode at the reflected port Φ_r and at the transmitted port Φ_t of the beam splitter have been measured by Carsten Heidemann to calculate the ratio $R_{r/t}$.
It is important to know that this ratio is wavelength dependent. During a measurement only $\Phi_{pin,t}$ can be measured. With $\Phi_{pin,t}$ it is possible to calculate the intensity at the reflected port.

$$\Phi_r = \Phi_t \cdot R_{r/t}(\lambda) = I_{0,r}(d_{pin}) \cdot F_{pin}(d_{pin}, NA) \tag{4.14}$$

$$\Phi_t = I_{0,t}(d_{pin}) \cdot F_{pin}(d_{pin}, NA) \tag{4.15}$$

$$I_{0,r}(d_{pin}) = \frac{\Phi_{pin,t}}{F_{pin}(d_{pin}, NA)} \cdot R_{r/t}(\lambda) \tag{4.16}$$

Now it is possible to calculate the total flux out of the fibre to the SiPM at the reflected port with $F_{full}(d_{pin}, NA)$.

$$\Phi_{total,r} = \frac{\Phi_{pin,r} \cdot R_{r/t}(\lambda)}{F_{pin}(d_{pin}, NA)} \cdot F_{full}(d_{pin}, NA) \tag{4.17}$$

With $\Phi_{total,r}$ it is possible to calculate $I_{0,r}(d_{sipm})$ and finally the flux on the SiPM:

$$I_{0,r}(d_{sipm}) = \frac{\Phi_{total,r}}{F_{full}(d_{sipm}, NA)} \tag{4.18}$$

$$= \frac{\Phi_{pin,t} \cdot R_{r/t}(\lambda)}{F_{pin}(d_{sipm}, NA)} \cdot \frac{d_{pin}^2}{d_{sipm}^2} \tag{4.19}$$

$$\Phi_{sipm}(d_{sipm}, d_{pin}, NA, a) = F_{sipm}(d_{sipm}, NA, a) \cdot I_{0,r}(d_{sipm}) \tag{4.20}$$

$$= c_{geom} \cdot \Phi_{pin,t} \cdot R_{r/t}(\lambda) \tag{4.21}$$

$$c_{geom} = \frac{erf\left(\frac{a \cdot b^2 \cdot \sqrt{1-NA^2}}{2 \cdot d_{sipm} \cdot NA}\right)^2}{1 - \exp\left(\frac{-b^4 \cdot (1-NA^2) \cdot R_{pin}^2}{d_{pin}^2 \cdot NA^2}\right)} \tag{4.22}$$

With the values from Table 2 for the different parameters it is possible to calculate the geometry factor. The distance d_{bt} is the addition from the thickness of the circuit board and the distance from the sensitive surface of the SiPM to the backside taken from the data sheet [20] [17].

parameter	value	error
NA	0.22	0.002
d_{pin} / mm	59.75	0.05
$d_{sipmback}$ / mm	59.75	0.05
d_{bt} / mm	2.56	0.3
d_{sipm} / mm	57.19	0.3
b*	1.730	-
a** / mm	6.0	-

Table 2: Values for calculating the geometry factor [17, 20]. * The value b is given in [20] and ** a is given in [17] in a sketch without any error.

Finally the geometry factor calculates to $c_{geom} = 0.579 \pm 0.008$. This value is important for the analysis of the dynamic range because the calculation of the photon flux depends on this value.

4.3.1 Approximation of the photon flux on the outer cells of the SiPM

With the Gaussian beam profile from the fibres it is quite impossible to guarantee a homogeneous photon flux over the SiPM.
An inhomogeneous photon flux makes the dynamic range measurement quite difficult because it is not possible to guarantee that every single cell receives a hit with the same probability. This makes it hard to show the upper limit of the dynamic range.

The easiest way to make the light fluxes homogeneous is to place the SiPM in a greater distance from the fibre but this is not possible in the optical test set-up. This section will show the different light fluxes between the inner area of the SiPM in comparison with the outer.

For this approximation the following integral have to be solved for different ranges.

$$F_{sipm} = \int\int \exp\left(\frac{-\sqrt{x^2+y^2}^2}{[d_{simp}\cdot\tan(\sin^{-1}(NA))/b^2]^2}\right) dxdy \tag{4.23}$$

With the values from Table 2 the exponent of the exponential function can be simplified to $\frac{-\sqrt{x^2+y^2}^2}{18.57}$.
The exact value for the denominator of the exponent is 18.57 ± 0.63.
For the approximation two different grids are used which are shown in Figure 4.8
The first grid is just an easy subdivision of the SiPM. The grid areas are evenly distributed around the center. The central point with the peak of the Gaussian profile occurs in the four central grid areas with A1. In the second grid the central grid area of the approximation equals an SiPM with an active area of $1 \times 1\,mm^2$. It can be approximated that the photon flux on this area is almost homogeneous. This approximation is good to see the different light fluxes on the outer areas of different SiPM sizes. For the flux integral the values are presented in Table 3.

A1	0.965	B1	0.991	C1	0.331
A2	0.867	B2	0.940	C2	0.314
A3	0.780	B3	0.891	C3	0.201
A4	0.701	B4	0.801	Corner	0.111
A5	0.630	B5	0.759		
A6	0.509	B6	0.647		

Table 3: Values of the flux integral for the different areas of the two approximations for the SiPM

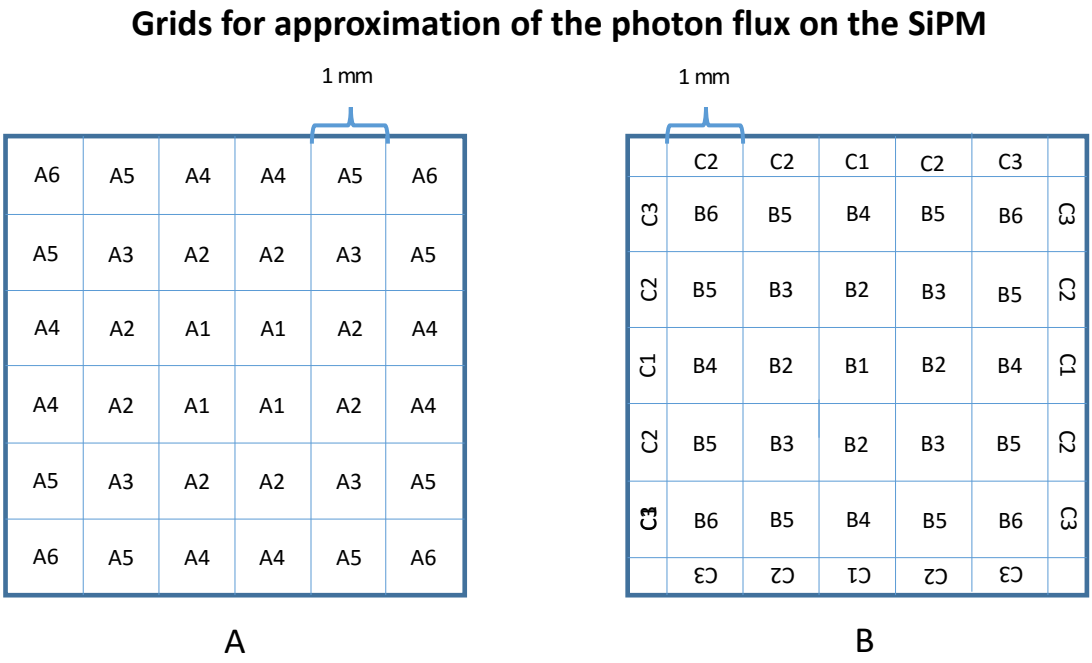

Figure 4.8: Two different grids for the approximation of the photon flux of the different areas of the SiPM.

From the values it can be seen that the inner area of the SiPM sees twice as much photons as the outer areas. Calculating the flux for every single cell is not as good as it seems because the position of the SiPM on the circuit board and the position of the circuit board inside the SiPM holder is not that well known.
So it can not be said that the center cell with a size of 25 μm or 50 μm is that exact in the middle. Also it can not be said if the SiPM is tilted so that the distance between the fibre and the cell is not equal for all the cells which gives an unpredictable error. These approximations got an error that is much greater than the uncertainty of the tilt so that the error from the tilt can be unattended.

5 Breakdown voltage and quenching resistor

To use SiPMs it is important to know the exact breakdown voltage of a SiPM. The reasons are described in a previous chapter. There are several different ways to measure the breakdown voltage, in this thesis only one is presented. It is noted that the different methods returns slightly different results for the breakdown voltage.

5.1 Measuring method and determination of the breakdown voltage

The method here presented, to determine the breakdown voltage is known as the current method. In this method the SiPM is illuminated with a continuous high light flux. LED 10 is used in this measurement.
During the measurement the bias voltage that lays on the SiPM will be increased from 48 V to 54 V in Steps of 0.1 V. Simultaneously the current flux from the SiPM is measured. Every current value is an average value of ten measured values. This is done to minimize the noise and other fluctuation of the current measurement.
From this data the relative current change per voltage $c_{rel}(V)$ is calculated [20].

$$c_{rel}(V) = \frac{dI}{dV} \cdot \frac{1}{I} \tag{5.1}$$

$$c_{rel}(n) = \frac{I(n+1) - I(n-1)}{V(n+1) - V(n-1)} \cdot \frac{1}{I(n)} \tag{5.2}$$

The parameter n represents the discrete point where the relative change is calculated. This is used because there are only discrete points that are measured and so the relative change can just be calculated numerically. In this calculation the two values next to the observed value are used to calculate the relative change.
There are also two different relative changes calculated for the discrete point n. These are c_{rel+} and c_{rel-}. In this calculations the discrete value and the value above or under the observed value are used.

$$c_{rel+} = \frac{I(n+1) - I(n)}{V(n+1) - V(n)} \cdot \frac{1}{I(n)} \tag{5.3}$$

$$c_{rel-} = \frac{I(n) - I(n-1)}{V(n) - V(n-1)} \cdot \frac{1}{I(n)} \tag{5.4}$$

These two parameters are calculated because the peaks in the $\frac{dI}{dV \cdot I}$ are higher, seen in Figure 5.1.

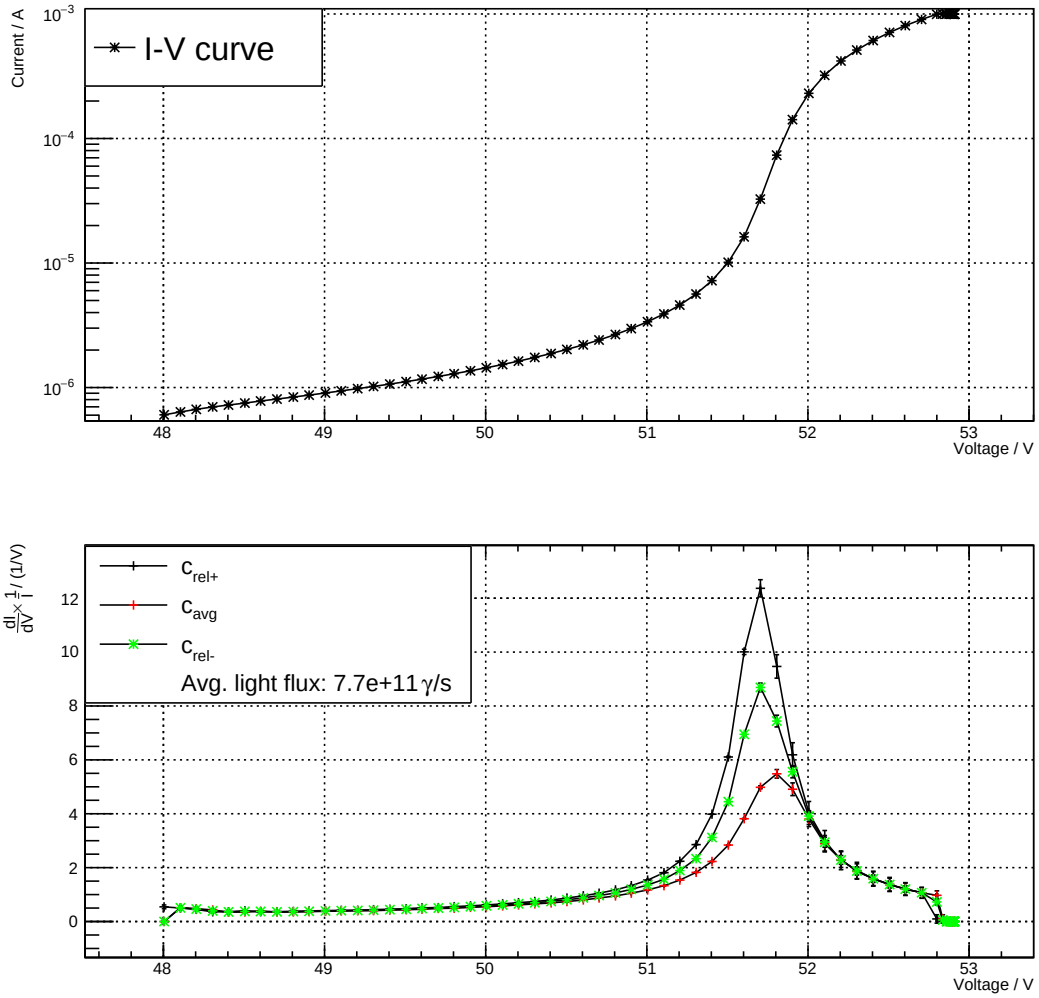

Figure 5.1: I-V-curve scan for calculating the breakdown voltage in the upper half of this figure. In the lower part the $\frac{dI}{dV} \cdot \frac{1}{I}$ plotted against the bias voltage is shown.

These large peaks in the derivative are scanned to determine a possible position of the breakdown voltage. Around a range of $\pm 1\,V$ around this averaged position of the two larger peaks a finer I-V scan is accomplished. This time the step size for the SiPM voltage is $0.01\,V$.
This time the calculated relative changes are fitted around the peak position with a Gaussian and the peak position is determined. This peak position corresponds to the

breakdown voltage. The other two calculated and fitted curves are used to estimate the error.

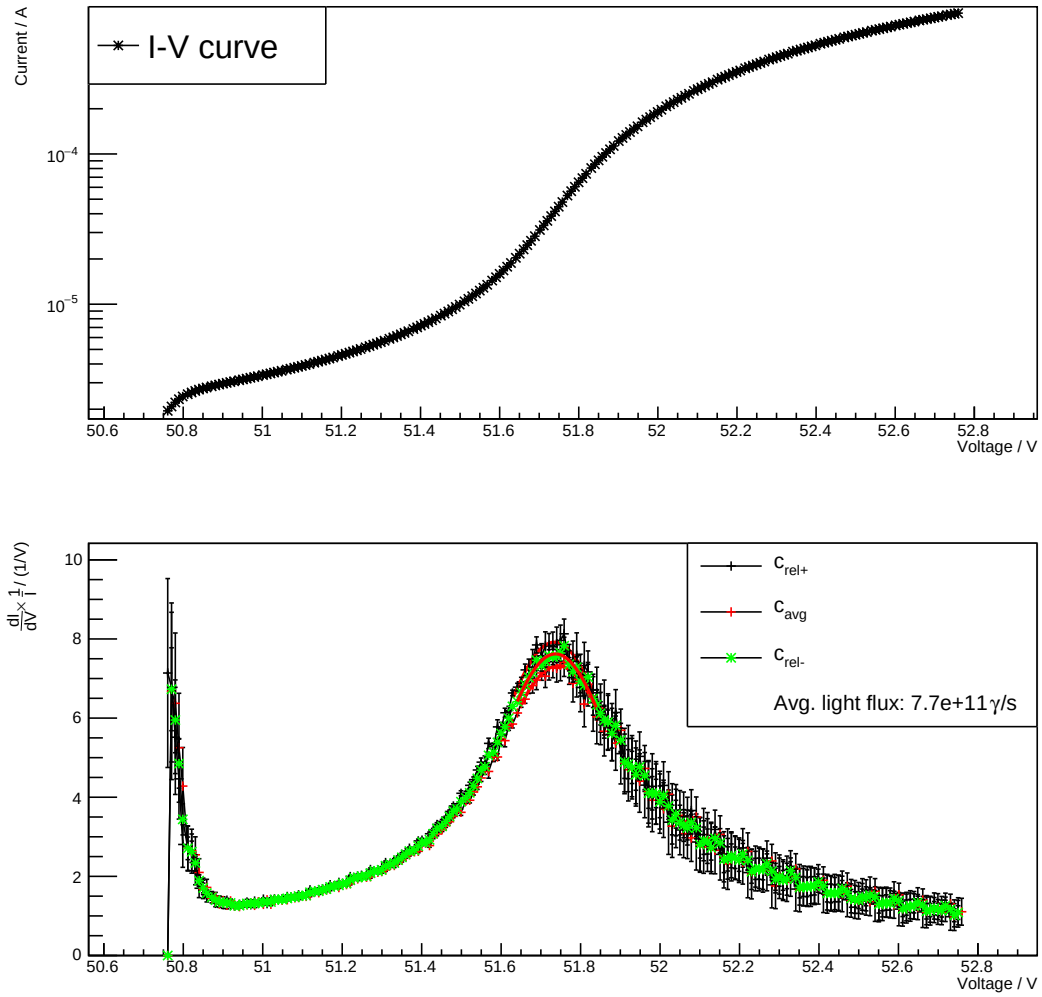

Figure 5.2: Fine scan of the I-V-curve from the 50 μm SiPM at 25 °C for calculating the breakdown voltage in the upper half. In the lower part the calculated $\frac{dI}{dV} \cdot \frac{1}{V}$ plotted against the bias voltage is shown.

By doing this measurement with different temperatures it is possible to determine the temperature dependency of the breakdown voltage. This measurement is done in temperature steps of 1 K in the temperature range between 15 °C and 30 °C.

For the whole temperature range from -25 °C up to 40 °C of the experimental set up this measurement is also done in steps of 1 K. The whole temperature range is measured at the end of all the measurements because the impacts of the lower temperature below the dew point could not be estimated. That means that it was possible that the water which is condensed inside the set-up could damage the SiPM.

The temperature dependency with fit for the measurement over the whole temperature range is shown in Figure 5.3 for the 25 μm and in Figure 5.4 for the 50 μm SiPM.

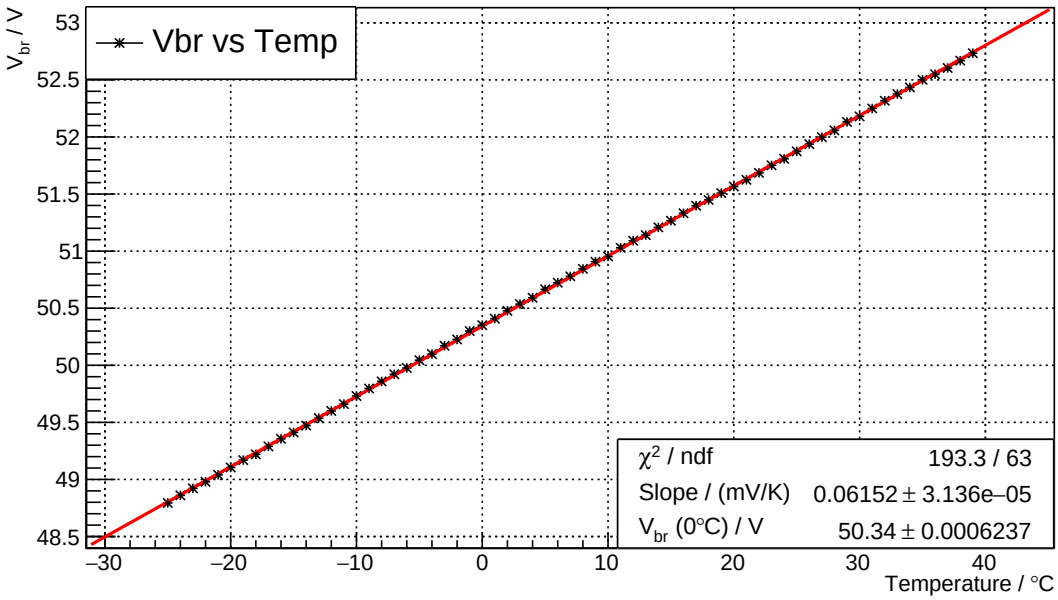

Figure 5.3: Breakdown voltage plotted against temperature for the 25 μm SiPM.

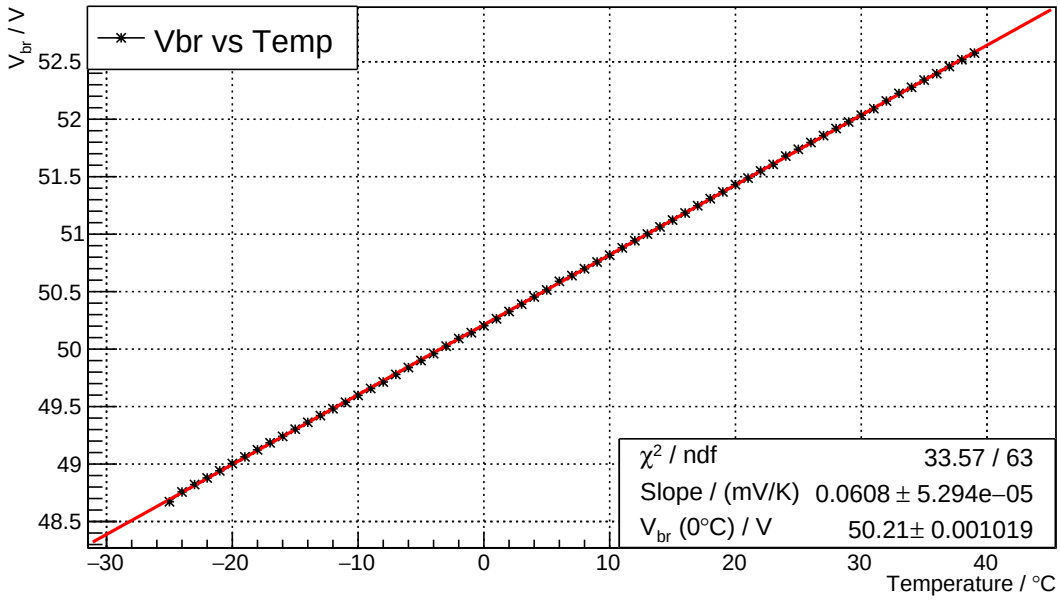

Figure 5.4: Breakdown voltage plotted against temperature for the 50 μm SiPM.

For the dynamic range measurement the values from the linear fit are used which are presented in Table 4.

SiPM	$\beta\,/\,(mV/K)$	V_{br} (25 °C) / V
25 μm	61.52 ± 0.04	51.880 ± 0.008
50 μm	60.79 ± 0.05	51.7317 ± 0.0016

Table 4: β-factor of the temperature dependency from the fit of the breakdown voltage against temperature plot and breakdown voltage at 25 °C.

The manufacturer gives for the breakdown voltage and temperature dependency the values presented in Table 5.
There are also values from three other SiPM manufacturers presented. At first it is easy to see that the breakdown voltage of the 25 μm SiPM and the temperature dependency of both SiPMs of the measurement disagree with the values from Hamamatsu, which perhaps is caused down to the fact, that Hamamatsu could have used a different method. Furthermore Hamamatsu do not elaborate the error on their data. The breakdown voltage of the 50 μm SiPM fits quite good to the data from the Hamamatsu datasheet [17].

One other thing that attracts attention is, that the value of the temperature dependency of the breakdown voltage could cohere with the value of the breakdown voltage. The higher the breakdown voltage the higher is the temperature dependency which could be compared with the values of the SiPMs from the other manufacturers. This could explain why the temperature dependency of the $25\,\mu m$ SiPM is a little bit higher than the temperature dependency of the $50\,\mu m$ SiPM. A possible correlation of the breakdown voltage and the temperature dependency of the breakdown voltage could explain that.

SiPM	V_{br} 25 °C / V	β / $(mV$ / $K)$
Hamamatsu $25\mu m$	52.17 ± 0.2	54
Hamamatsu $50\mu m$	51.73 ± 0.2	54
SensL 60035	24.45 ± 0.25*	21.5
ASD-NUV3S-P	26 ± 2*	26
Excelitas C30742-66-55-C	95 ± 0.2*	90

Table 5: Values for the temperature dependency and the breakdown voltage at 25 °C for the two studied SiPMs given by Hamamatsu [17] and from not studied SIPMs from SensL [21], AdvanSiD [22] and Excelitas [23]. The values with * are values from data sheet. That means that the difference between two SiPMs could be greater than the given error. The values of Hamamatsu are the especial values for this two SiPMs.

5.2 Errors by measuring the breakdownvoltage using the I-V-curve

The protective resistances of the optical test set-up and the quenching resistance of the SiPM influence the I-V-curve measurement of the breakdown voltage. The breakdown voltage that is calculated in the previous section is already corrected by this resistances. In this section the calculation of these values and the impact of these resistances is shown.

To calculate the quenching and the protective resistance on the circuit board from the optical test set-up different I-V-curves in forward direction of the SiPM and a I-V-curve with a wire instead of a SiPM are measured. The wire is used to calculate the protective resistance on the circuit board because in every measurement of the quenching resistance, the protective resistors have a great impact on the measurement.

For an exact measurement the temperature dependency of the quenching resistance and the protective resistance has to be known. For this temperature dependency the I-V-curves for different temperatures are measured and analysed.

Figure 5.5: Board with protective resistance [20].

Protective resistance

At first the calculation of the protective resistance is shown because the calculation of the quenching resistance depends on the protective resistance.

The I-V-curve of at a temperature of 25 °C is shown in Figure 5.6.
It is easy to see that the curve follows Ohm's law: $U = R \cdot I$. U is the voltage, R the value of the resistance and I the current.

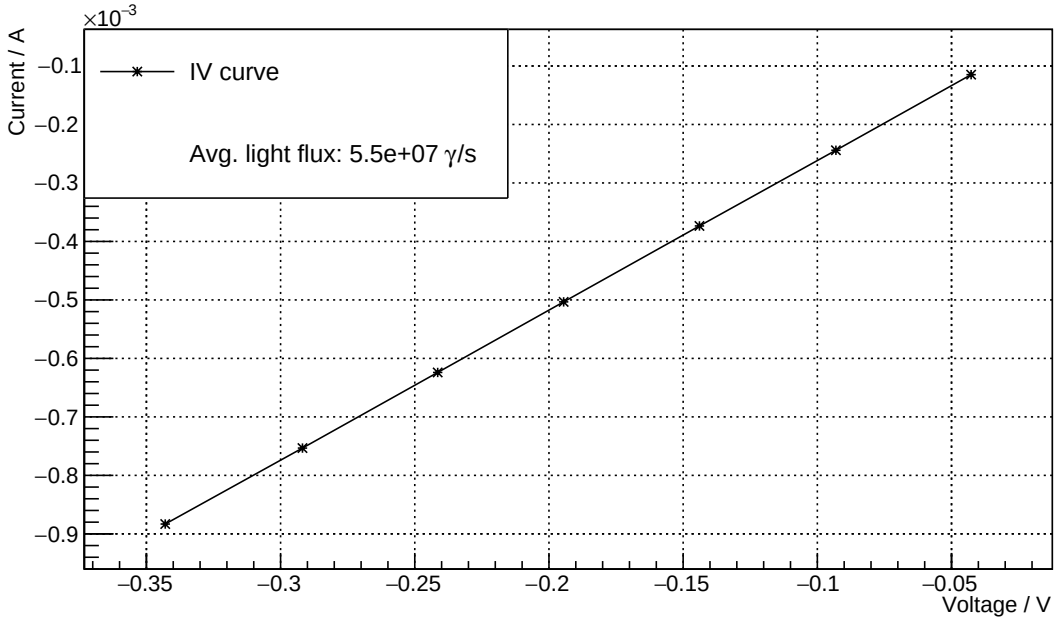

Figure 5.6: I-V-curve of the protective resistance in forward direction at 25 °C with fit.

The shown curve will be fitted by a straight line. The slope of the fitted curve equals $\frac{1}{R}$.

To calculate the temperature dependency of the protective resistance, I-V-curves in a range between 15 °C nd 30 °C are measured in temperature steps of $\Delta T = 1\,K$.

All the fits have nearly the same slope and the same offset, so that they are located all above each other and it is hard to separate them in one plot. In Figure 5.7 the values for the calculated resistance are plotted against the temperature.

It is easy to see that there is no ordinary temperature dependency. That was expected because the circuit board with the protective resistance is located in the isolated area of the test set-up but it is not directly connected to the cooled or heated copper mass.

The linear fit in Figure 5.7 is just the average value of the protective resistance.
The protective resistance is calculated to $(390.574 \pm 0.014)\,\Omega$ with $\chi^2 \,/\, \mathrm{ndf} = 14.43 \,/\, 15$.

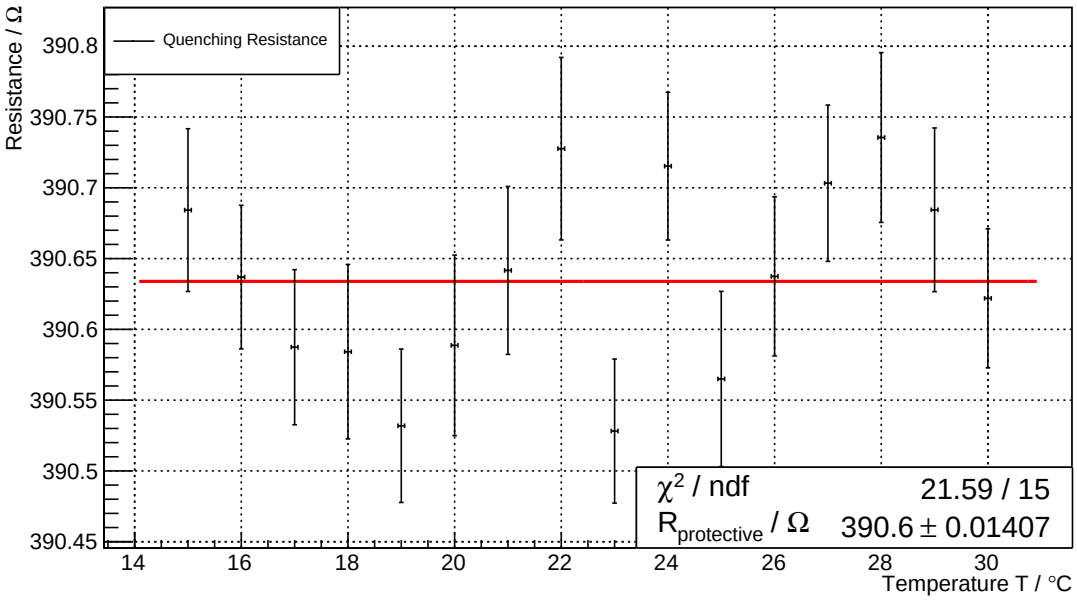

Figure 5.7: Protective resistance plotted against temperature to identify the temperature dependency with average fit.

Quenching resistance

For the calculation of the quenching resistance I-V-curves for different temperatures are measured. The I-V-curve in forward direction at 25 °C is shown in Figure 5.8.

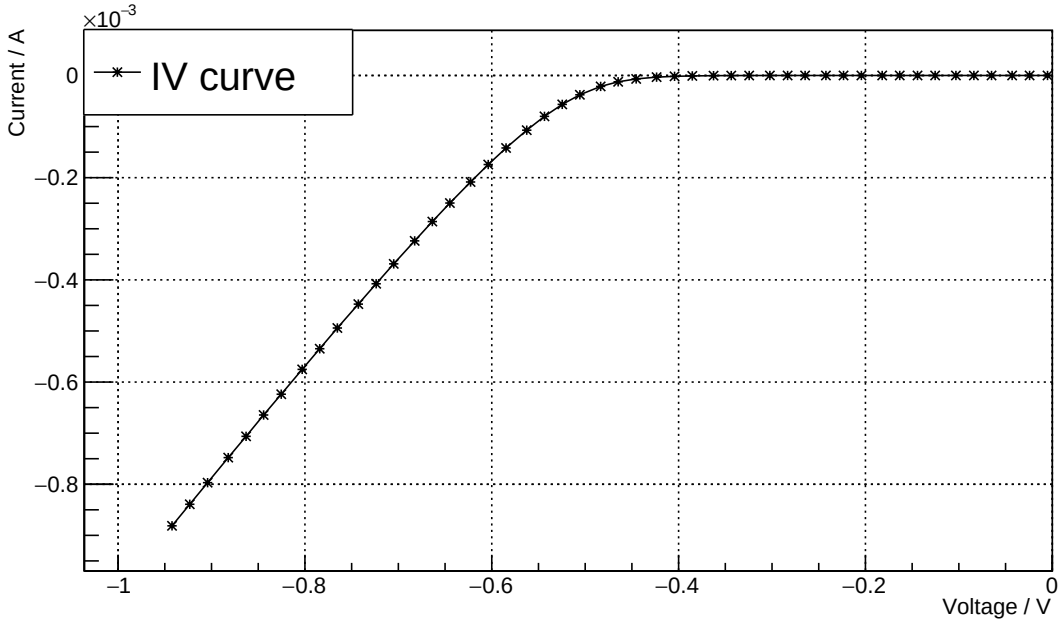

Figure 5.8: I-V-curve in forward direction of the 50 μm SiPM at 25 °C

To calculate the total resistance* the linear part at the end of the I-V-curve is fitted. The non linear part of the I-V-curve is the part where the voltage on the SiPM can not defeat the barrier layer and the current increases non linear because the impact of the barrier layer decreases. When the voltage on the SiPM is that high, that there is no barrier layer any more, the current increases linear with Ohm's law. For these fits it is important to have a fit range that just includes the linear part because this is the part where Ohm's law is applied. In this analyse the fit range is between $-0.95\,V$ and $-0.8\,V$. The slope of the fit equals $\frac{1}{R}$ like in the measurement of the protective resistance.

To calculate the temperature dependency I-V-curves in a temperature range between 15 °C and 30 °C are measured and fitted. These curves for the 50 μm SiPM are plotted in Figure 5.9 and for the 25 μm SiPM in Figure 5.10.

*Total resistance means the linear combination of protective and quenching resistance because it is just possible to measure this total resistance. That is the reason why the protective resistance has also been measured.

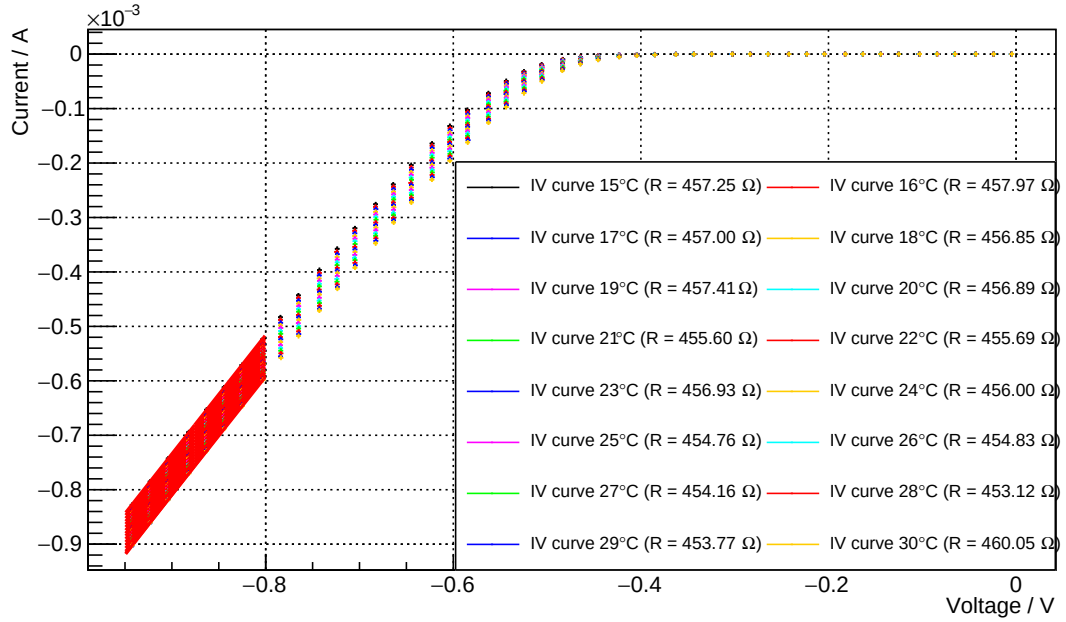

Figure 5.9: Combination of all I-V-curves and fits of the 50 μm SiPM for a temperature range from 15 °C to 30 °C

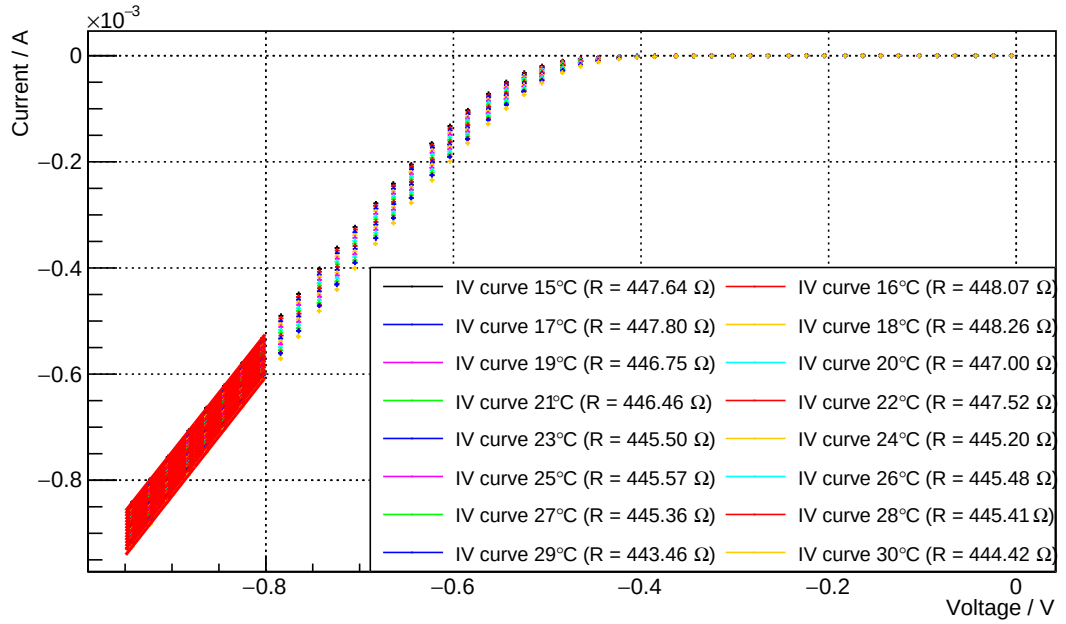

Figure 5.10: Combination of all I-V-curves and fits of the 25 μm SiPM for a temperature range from 15 °C to 30 °C

The resistance values are the values for the resistance of the whole circuit. This means quenching and protective resistor in a series combination.

After subtracting the protective resistance with a value of $(390.57 \pm 0.014)\,\Omega$ it is possible to plot the quenching resistance against the temperature. The plotted values of the quenching resistance are the values of the parallel combination of all the micro-cells. That means that the value of one quenching resistance is the number of cells multiplied with the total quenching resistance. This is easy to calculate with

$$\frac{1}{R_{Q-total}} = \sum_{n}^{number\ of\ cells} \frac{1}{R_{Q_n}}.$$

The temperature dependency of the quenching resistance of the 25 μm SiPM is presented at Figure 5.11 and from the 50 μm SiPM in Figure 5.12.
The quenching resistance of one cell at a temperature of 25 °C and the results from the two fits are presented in Table 6

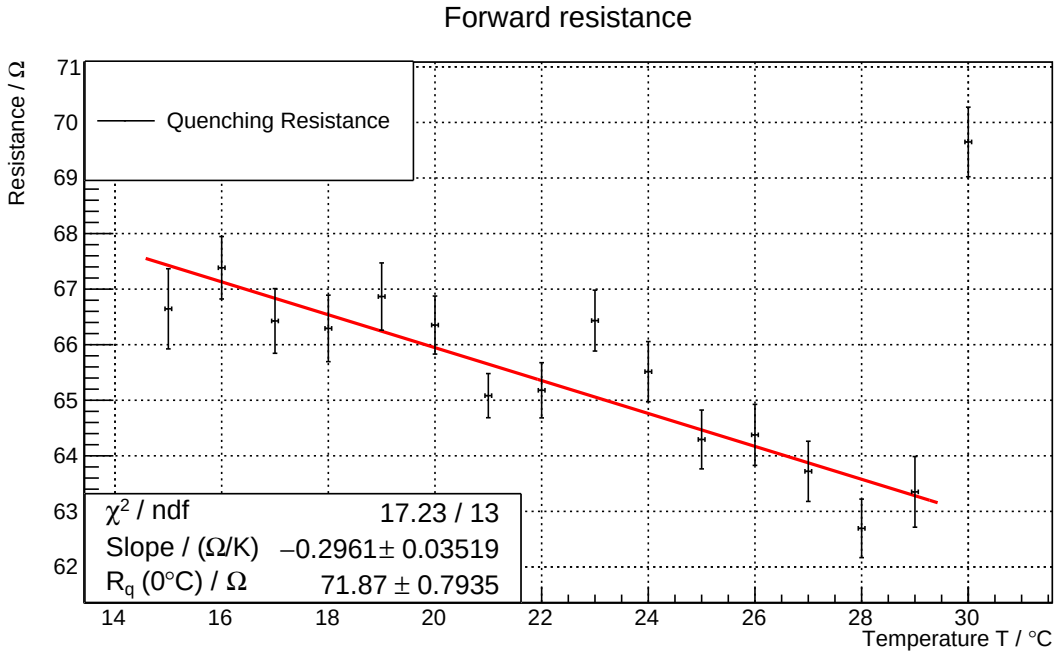

Figure 5.11: Total quenching resistance of the 50 μm SiPM against temperature plotted with linear fit.

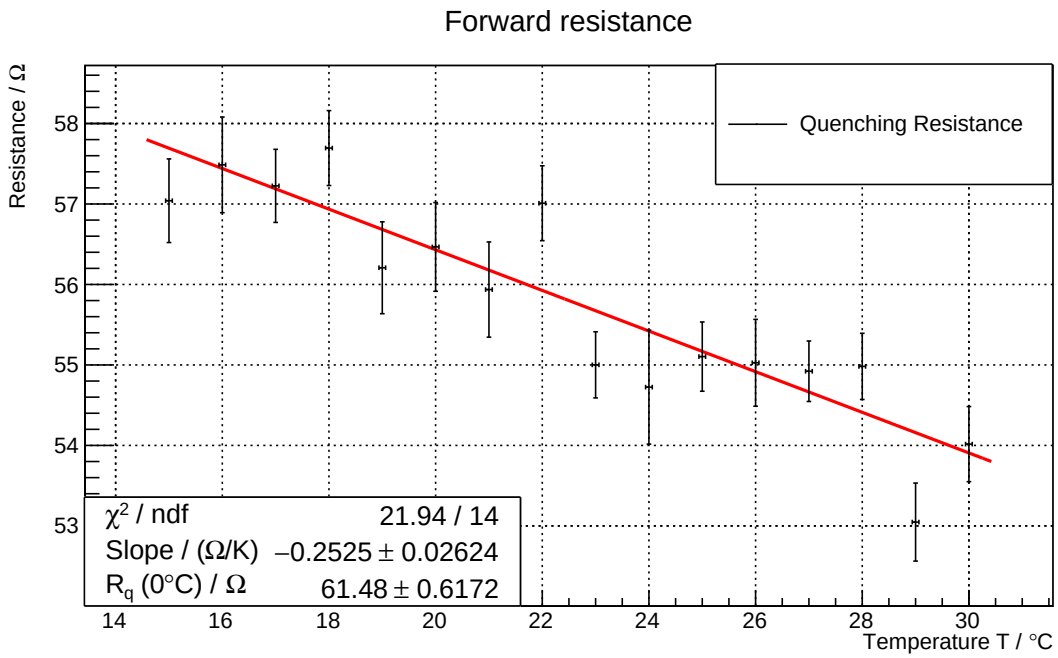

Figure 5.12: Total quenching resistance of the 25 μm SiPM against temperature plotted with linear fit.

SiPM	$R_Q\,(25\,°C)\,/\,\Omega$	$\beta_{R_Q}\,/\,(\Omega\,/\,K)$
25 μm	$(3.121 \pm 0.007) \times 10^6$	$(-15.0 \pm 1.4) \times 10^3$
50 μm	$(0.9239 \pm 0.0008) \times 10^6$	$(-4.3 \pm 0.4) \times 10^3$

Table 6: Fit results and quenching resistance at 25 °C

It is easy to see that the assigned value for the resistance at a temperature of 30 °C for the 50 μm SiPM failed. The fit range for the 50μm SiPM is from 15 °C up to 29 °C.

These quenching and protective resistance shifts the I-V curve of the breakdown voltage measurement. To determine the exact I-V-curve with just the impact of the SiPM the current over the protective and the quenching resistance has to be calculated with Ohm's law and subtracted from the measured current. This current depends of the bias voltage.

The relative impact depends on the measured current. An example calculation will show the impact of this resistances.
At a voltage of 51.9 V a current of $\sim 10^{-4}\,A$ is measured, seen in Figure 5.1. That means that there is an resistance of the SiPM from $\sim 519\,k\Omega$. When the quenching and the

protective resistance will also influence this measurement we have a total resistance of $\sim 590,500\,\Omega$. That means that the current will be calculate to: $\sim 0.99903\,A \approx 10^{-4}\,A$. The effect of the quenching and the protective resistance is smaller than 0.1%

6 Dynamic range measurement

In this chapter the dynamic range measurements for the Hamamatsu SiPMs are presented. At first the measurement method used in the optical test set-up for the dynamic range will be described. Then the different analyses that are made in the test set-up and a new implemented analyses will be presented. At last the temperature dependency of the dynamic range is measured for two different temperatures with adapted breakdown voltage.

6.1 Measuring and data analyses methods

The dynamic range measurement could be done with the high voltage (HV) pulsed LEDs as well as with the DC LEDs with an external pulser. The LED will be pulsed with a frequency of $10\,kHz$ if it is a Hv pulsed LED. In the shown measurement just the HV pulsed LEDs are used because with them is is possible to generate higher photon fluxes and shorter light pulses.
To increase the number of photons, that light up the SiPM, the voltage of the pulser has to be increased. With the measured flux on the PiN diode the photon flux on the SiPM can be calculated. The formula was derived in a previous chapter but for a better understanding it will be presented here again [20].

$$\Phi_{sipm}(d_{sipm}, d_{pin}, NA, a) \;=\; c_{geom} \cdot \Phi_{pin,t} \cdot R_{r/t}(\lambda) \tag{6.1}$$

With $R_{r/t} = 1.140$ [20] for LED number 9 and 10 and $c_{geom} = 0.579 \pm 0.008$.
The peak wavelength of the LEDs amounts: $\lambda_{9/10} = 460\,nm$, see Figure 4.3.
The SiPM signal is measured with the oscilloscope and the sourcemeter. With the sourcemeter the average current from the SiPM is measured.
Another measurement method is to measure short traces with the oscilloscope. From this short traces it is possible to calculate the SoftQDC data what will be explained later. After every measurement a dark measurement is done to calculate a dark count correction. This is also done with the sourcemeter and the oscilloscope.

SiPM flux analyses

With the measured current it is possible to calculate the fired cells. At first the current will be corrected with the current of the dark measurement. This is important because the SiPM have a dark count rate which will introduce a current offset. After subtracting

the dark current it is possible to calculate the number of fired cells.

$$N_{fired} = \frac{\text{SiPM current corrected * Cuolomb}}{\text{SiPM gain} \cdot \text{frequency}} \tag{6.2}$$

The division by the frequency of the pulser is necessary to calculate the number of fired pixel per pulse. The determination of the gain is done with the photon equivalent (pe) charge. This will be described later in this chapter.

Short traces and SoftQDC data analyses

The segment memory function of the oscilloscope allows a fast acquisition of triggered traces. They contain the desired signal what is a great advantage. An example of the SoftQDC charge determination is given in Figure 6.1

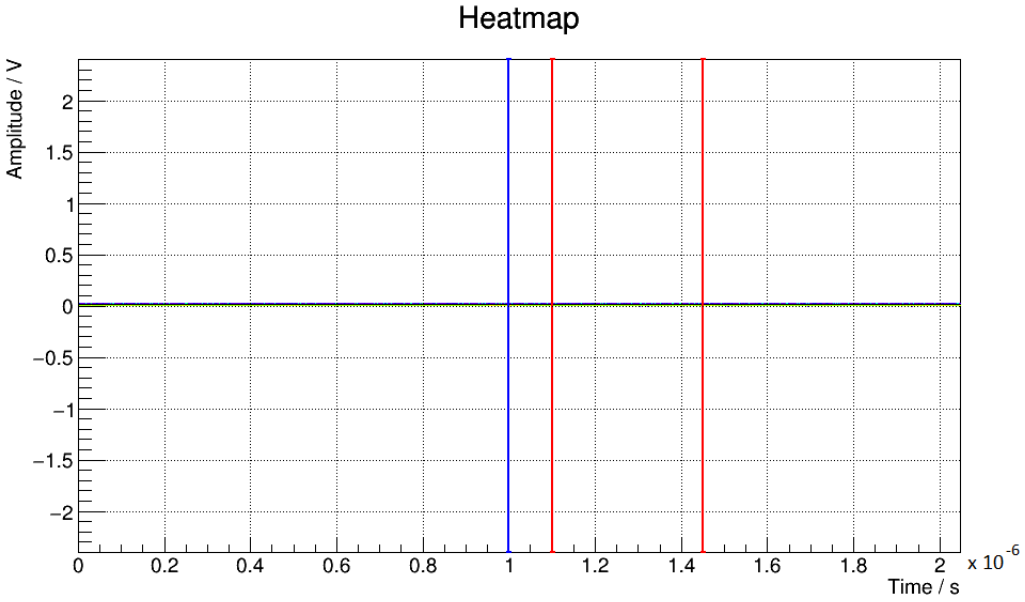

Figure 6.1: Example of the charge determination with short traces. The blue line indicates the trigger and the two red lines are the integration window.

The blue line identifies the trigger. Left from the trigger is the baseline window, which is used to determine the baseline.
After a short signal delay follows the integrations window between the two red. In case of the different signal run time the SiPM signal is delayed by a few nanoseconds and thus appears after the trigger of the trace.

The black line in the middle of the data illustrates the average data.
The charge of each short trace can be determined with a correction for a possible baseline shift by determining the average baseline level in the first half of the short trace [20].

$$Q_i = \frac{U_i - U_{avg.\,baseline}}{R \cdot M_{gain}} \cdot \Delta t \tag{6.3}$$

$$Q = \sum_{i=start}^{stop} Q_i = \frac{\Delta t \cdot (stop - start)}{R \cdot M_{gain}} \cdot \sum_{i=start}^{stop} (U_i - U_{avg.\,baseline}) \tag{6.4}$$

U_i represents the measured voltage, $U_{avg.baseline}$ is the average baseline level from the baseline window. Start and stop represents the start and stop time bin for the integral, Δt the time bin width.

The value R is the input impedance of the oscilloscope $R = 50\,\Omega$ [20]. In the optical test set-up the oscilloscope measures in parallel to an resistance.

A schematic of the positioning of the oscilloscope parallel to the additional resistance is shown in Figure 6.2. The oscilloscope is coupled over a coupling capacitor.

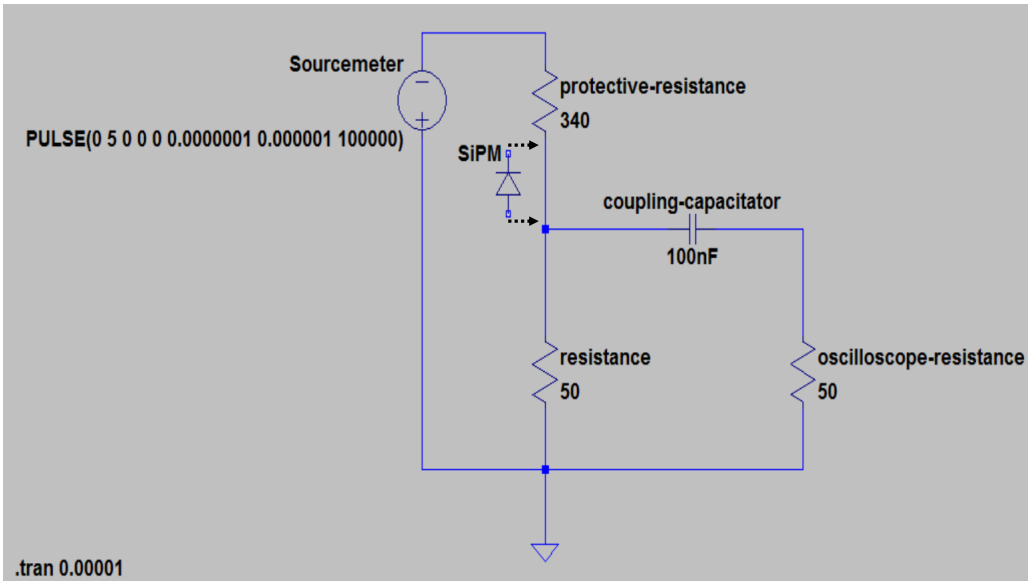

Figure 6.2: Circuit of the determination of the impact of the additional resistance parallel to the oscilloscope measurement.

To determine the impact of the coupling capacitor on the oscilloscope measurement a LTSpice simulation of the circuit represented shown in Figure 6.2 is done with voltage

pulses of 5 V with a length of 0.1 μs is done. The result of the simulation is shown in Figure 6.3

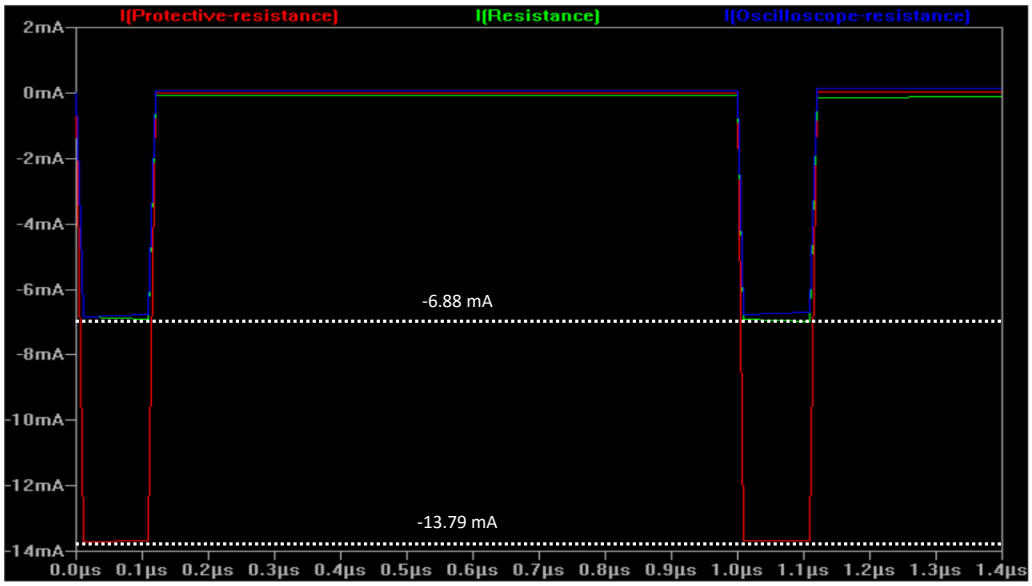

Figure 6.3: Simulation of the current flux over the three different resistors. The current at the protective resistor equals the current measured at the sourcemeter. The current at the other two resistors represents the current at the oscilloscope and the not measured current.

It is easy to see that the oscilloscope just measures the half of the signal that is measured at the sourcemeter.
To recalculate this effect the resistance in the formula for the calculation of the charge must be the resistance of the parallel connection of the two resistors. The two resistors have the same resistance, it is easy to calculate the new total resistance to $R_{total} = 25\,\Omega$.

The factor M_{gain} is just relevant if the measurement is done with an amplifier. In this measurement the factor equals 1 because no amplifier is used.

The calculated charges are filled into a histogram as seen in Figure 6.4. In the histogram three different data series are plotted, the raw QDC data, the baseline data and the corrected QDC data.

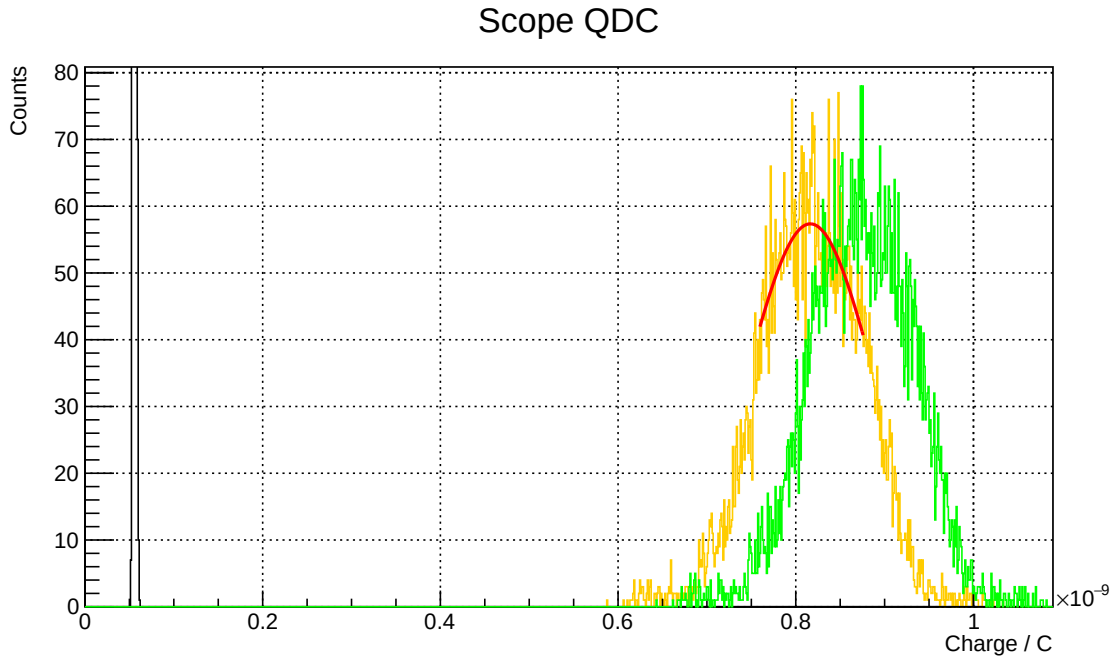

Figure 6.4: Example of the charge determination with SoftQDC. Green the uncorrected data, black the average baseline data, yellow the corrected data and red the fit for the meancharge.

With the corrected data and a Gaussian fit the meancharge of the SiPM pulse will be calculated. The number of fired cells can be calculated by the meancharge divided by the photon equivalent (pe) charge.

Determination of the photon equivalent charge

The photon equivalent (pe) charge is an important characteristic of the SiPM for measuring the dynamic range. With the pe charge the gain of the SiPM is calculated to use it in the SiPM current measurement to calculate the number of photons.
For the determination of the pe charge QDC histograms of a low light flux are recorded. For these low light fluxes LED 10 is used because it is possible to produce lower light fluxes with an lower pulser voltage than with LED 9. The advantage is that both LEDs have the same peak nearly the same peak wavelength at $\sim 460\,nm$ and a nearly same wavelength range. The problem is that the signal of the SiPM is quite noisy, what makes the determination of the pe charge highly complicated.
For the determination possible pe peaks of the QDC histogram are determined by hand because the algorithm from the test set-up could not do this and also no self made algorithm could estimate the peaks from the QDC histogram.
Every time the charge distance of two of these peaks is determined, because it was not

SiPM	$50\,\mu m$	$25\,\mu m$
pe charge / V	$(2.51 \pm 0.11) \times 10^{-13}$	$(1.08 \pm 0.05) \times 10^{-13}$
Gain	$(1.57 \pm 0.06) \times 10^{6}$	$(6.74 \pm 0.31)^{5}$
Gain Hamamatsu	1.7×10^{6}	7.0×10^{5}

Table 7: Results from the pe charge and gain determination and comparison with the value from the data sheet [17].

which pe peaks could seen. Furthermore this is done for QDC histograms with light fluxes where a higher number of pe could be seen and it was not clear which pe peak could seen. Also dark measurements are used to see small pe values.

Such a QDC histogram is shown in Figure 6.5.

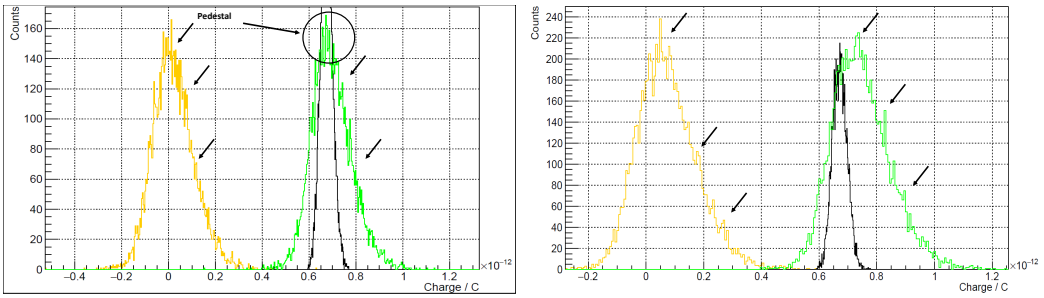

Figure 6.5: Two different determinations of the pe charge with QDC histogram with small light fluxes on the SiPM for $25\,\mu m$ SiPM.

From the values of the difference charge between two peaks an average value is determined. The error of the pe charge is the error of the average value. With this method it is possible to get a pe charge that is represented in Table 7.

Determination of the light pulse length

For a good understanding of the photon flux on the SiPM it is important to know the temporal extend of the light pulse from the SiPM. There are different methods to approximate the temporal extent. In this thesis the respond of the $25\,\mu m$ SiPM will be used to estimate the temporal extent. This is just an approximation in first order because it will be supposed that the recovery time of one cell is much smaller than the length of the light pulse.

The response at from the SiPM for a determination of the light flux can be seen in Figure 6.6. The green lines define the start and the end point of the SiPM pulse and

because of the small recovery time of the SiPM in proportion to the light pulse, the length of the light pulse.

In this approximation the pulse is nearly 250 ns long. In the first 100 ns between the first green and the yellow line, the pulse can be approximated as a uniform pulse. After the first 100 ns the pulse has an exponential decay. This decay is occurred by the afterglow of the LED. This exponential decay of the light flux continues for approximately 150 ns.

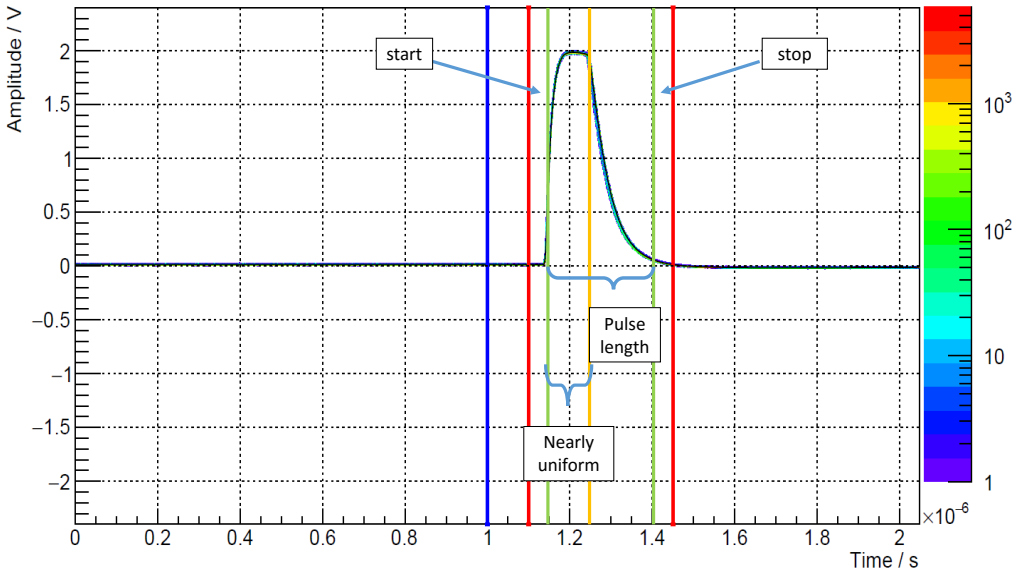

Figure 6.6: Determination of the light pulse length for high photon fluxes by determination of the SiPM response pulse length with the approximation that the recovery time of the SiPM cells is much smaller than the pulse length. The two green lines edge the total length of the pulse. Between the first green line and the yellow line the pulse can be approximated as uniform. The second part of the pulse occurs by an afterglow of the LED and has an exponential amount.

This widespread of the light pulse limits the dynamic range measurement which will be discussed in the discussion part of the dynamic range measurement.

6.2 Dynamic range analyses

The dynamic range measurements are done at a temperature of 25 °C. The measurements are done with light of an wavelength that is near to the peak wavelength of the PDE $\lambda_\gamma = 460\,nm$. The overvoltage of both SiPM is the overvoltage that is given by the manufacturer as operational overvoltage, that means for the 25 μm SiPM an

overvoltage of 5 V and for the 50 μm SiPM an overvoltage of 3 V. For the breakdown voltage the results from the chapter about the determination of the breakdown voltage are used. A possible temperature dependency will be presented in the following section.

The voltage of the LED is increased in steps of less than 1 V from 2.4 V up to 95 V. For the higher voltage areas the steps of the increasing are bigger in case of a smaller increase of photon flux per voltage. With an LED voltage of 95 V it is possible to have a photon flux up to 1.2×10^6 photons on the SiPM. A higher voltage is possible but it is not known at which voltage the LED will be destroyed and the increasing of the photon rate is that small that a higher voltage is not useful.

The results of the current data analyses is showed in Figure 6.11 for the 25 μm SiPM and in Figure 6.12 for the 50 μm SiPM.

The number of the detected photons calculated out of the QDC data analyses is at a higher photon level different to the current data. This is an effect of the integration window of the short trace data. The calculated photon flux of the short trace data shown in Figure 6.7 will be fitted to the current data analyses. The whole pulse indicated by the light is inside the integration window. In contrast the number of detected photons of the trace analyses is smaller than the number of photons of the current data because the integration window is smaller than the peak of the light signal like in Figure 6.8.

The integration window is 250 ns long as shown previous in this chapter. The 25 μm SiPM has a total recovery time of 20 ns and the 50 μm SiPM a total recovery time of 50 ns [12]. Total recovery time means the time until the cell is to 100% recovered and the pulse from an indicated photon has the same height as the pulse from a cell that has never been fired. In this time it is possible that a photon fires a cell but the pulse of the cell is not that high. The profile of the beam makes the calculation of the number how often a cell could be fired a little bit more difficult.

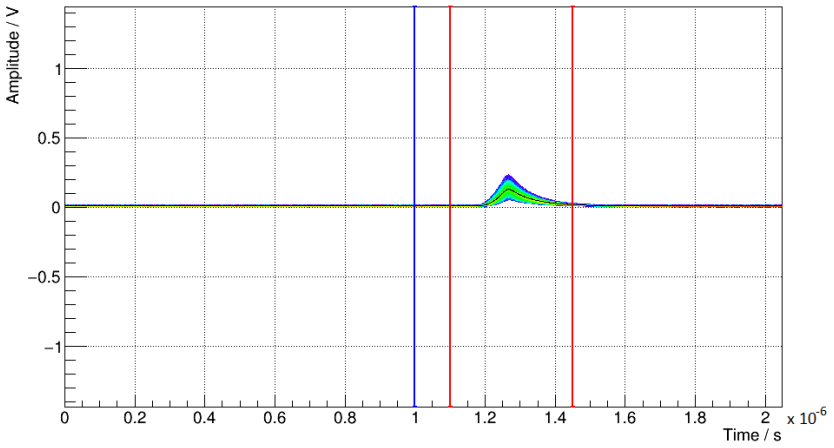

Figure 6.7: Short trace analyses with an integration window that fits with the pulse indicated by the light flux, of the 25μm SiPM at a wavelength of the incident photon of 460 nm and an overvoltage of 5 V.

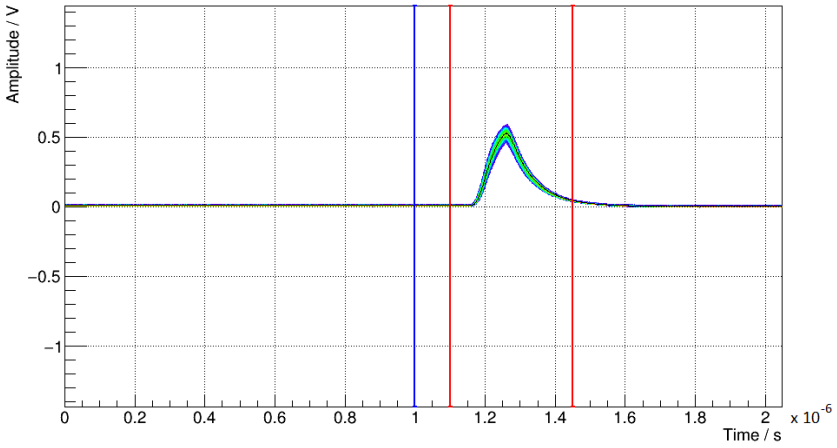

Figure 6.8: Short trace analyses with an integration window that is smaller than the pulse of the light flux, of the 25μm SiPM at a wavelength of the incident photon of 460 nm and an overvoltage of 5 V.

The integration error of the QDC data is larger for the 50 μm SiPM. This is caused by the smaller pulse of the 50 μm SiPM. The short traces with a LED voltage of 95 V for the 25 μm SiPM and the 50 μm SiPM are shown in Figure 6.9 and Figure 6.10. In this short trace analyses the larger part of the pulse outside the integration window

is seen. The calculated photons of from both analyses methods plotted against the incident photons calculated from with the current of the PIN diode are shown for the 25 μm SiPM in Figure 6.11 and for the 50 μm SiPM in Figure 6.12.

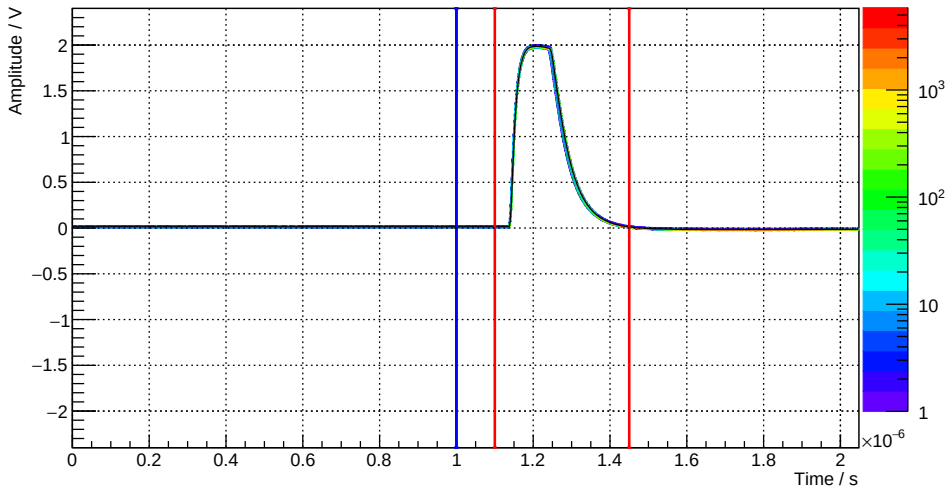

Figure 6.9: Short trace analyses for large number of photosn of the 25μm SiPM at a wavelength of the incident photon of 460 nm and an overvoltage of 5 V with an integration window that does not fit perfectly to the pulse length.

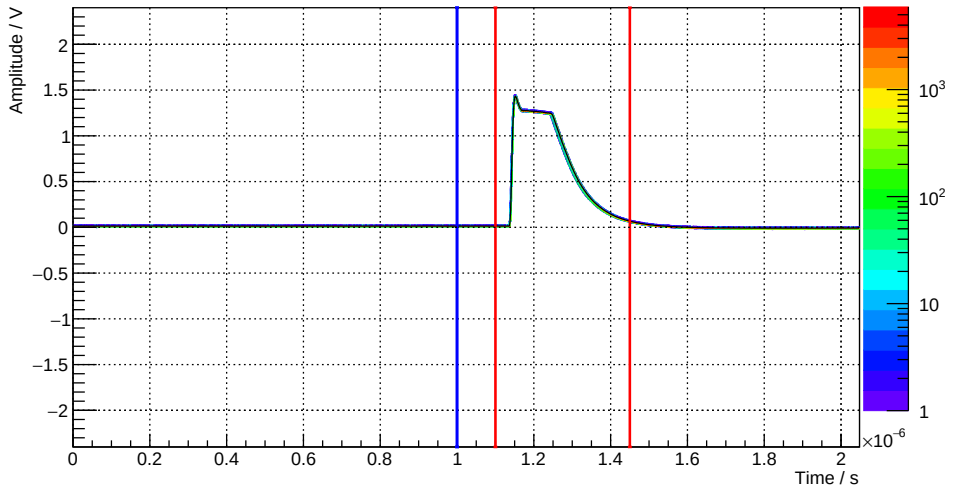

Figure 6.10: Short trace analyses of the 50 μm SiPM. The part of the light pulse outside the integration window is bigger than the part outside the integration window of the 25 μm SiPM.

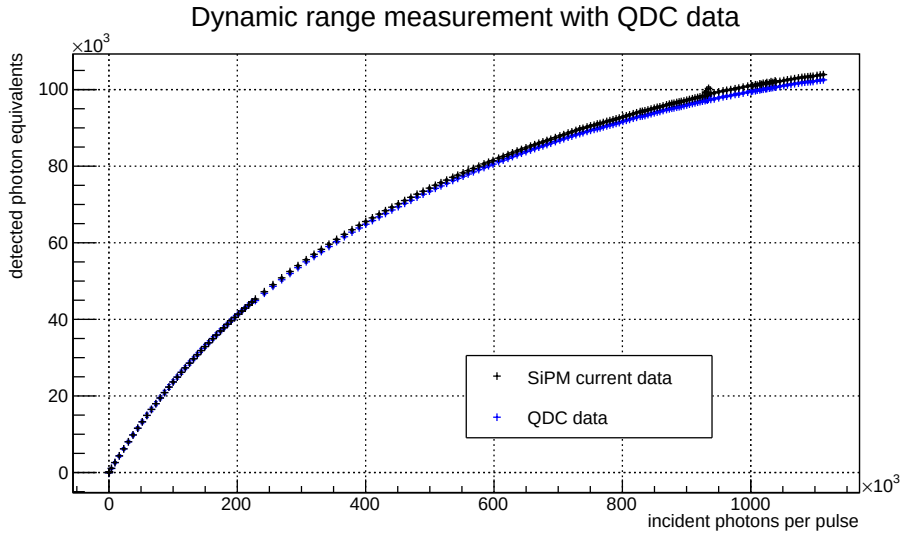

Figure 6.11: Detected photons plotted against incident photon analysed with the current of the SiPM with a cell pitch of 25μm and the short trace analyses at a temperature of 25 °C with an overvoltage of 5 V and a photon wavelength of $\sim$ 460 nm.

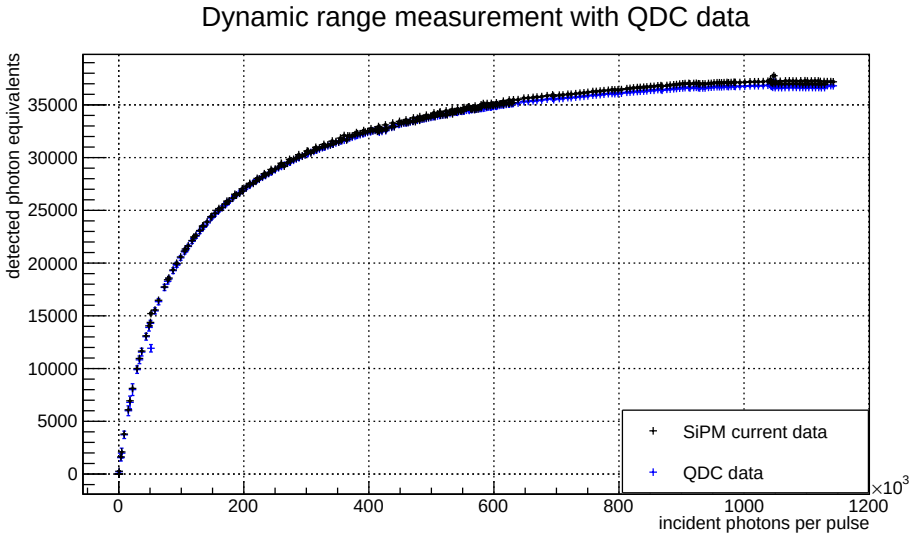

Figure 6.12: Detected photons plotted against incident photon analysed with the current of the SiPM with a cell pitch of $50\mu m$ and the short trace analyses at a temperature of 25 °C with an overvoltage of 3 V and a photon wavelength of $\sim 460\,nm$.

Photon Number Resolution

The photon number resolution is an easy way to compare the measured dynamic range of two measured SiPM. The comparability of the two measurements in the plot from the incident photons against the detected photons are limited. A plot with both dynamic range measurements is shown in Figure 6.13. It is hard to compare these plots in case of different number of cells and different characteristics of the SiPM.

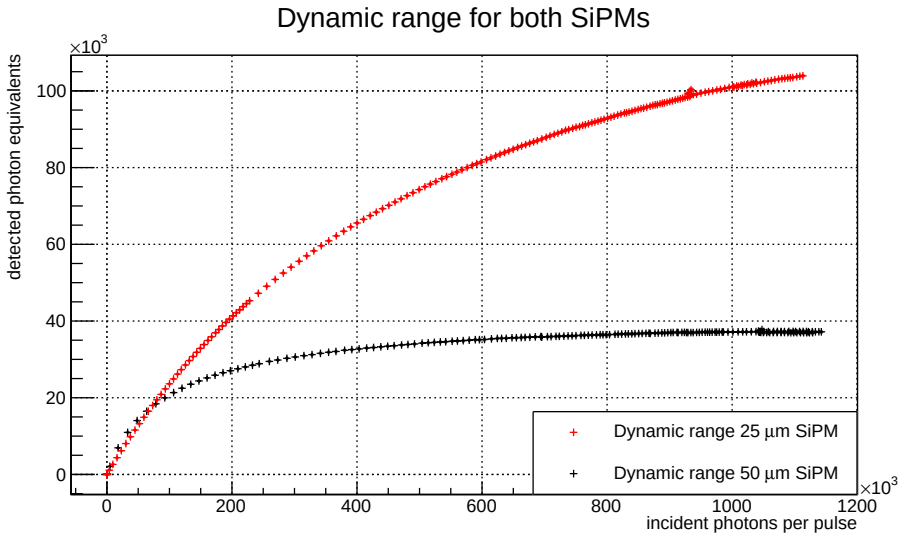

Figure 6.13: Dynamic range plot for both SiPM with an overvoltage of 5 V for the 25 μm SiPM and 3 V for the 50 μm SiPM at a temperature of 25 °C and a wavelength of $\sim 460\,nm$.

To compare the two SiPMs and to determine the dynamic range the photon number resolution will be calculated with the following formula.

$$\text{photon number resolution} = \frac{\sigma_{N_f}}{N_f} \times \frac{N_f(N_\gamma)}{N_\gamma} \times \frac{1}{\frac{dN_f(N_\gamma)}{dN_\gamma}} \tag{6.5}$$

N_f represents the number of fired cells, N_γ is the number of incident photons, σ_{N_f} is the error of the number of fired cells.

The formula for the photon number resolution can be derivated with the chain rule and describes the error of the incident photons when the number of detected photons is given.

$$\sigma(N_f(N_\gamma)) = \sigma(N_\gamma) \times \frac{dN_f(N_\gamma)}{dN_\gamma} \tag{6.6}$$

$$\frac{\sigma(N_f(N_\gamma))}{N_f(N_\gamma)} = \sigma(N_\gamma) \times \frac{dN_f(N_\gamma)}{dN_\gamma} \times \frac{1}{N_f(N_\gamma)} \times \frac{N_\gamma}{N_\gamma} \tag{6.7}$$

$$\frac{\sigma(N_\gamma)}{N_\gamma} = \frac{\sigma(N_f(N_\gamma))}{N_f(N_\gamma)} \times \left(\frac{dN_f(N_\gamma)}{dN_\gamma} \right)^{-1} \times \frac{N_f(N_\gamma)}{N_\gamma} \tag{6.8}$$

With this formula it is possible to calculate a dynamic range where the SiPM responds a useful output. It is possible to divide the formula in three different part.

The first part

$$\frac{\sigma_{N_f}}{N_f}$$

is the relative error of the number of fired cells. This part gives a lower bound of the dynamic range because the relative error in the lower part of the dynamic range is near to one because the error is in the same scale as the calculated number of cells. The relative error also scales the calculated photon resolution number to the error of the fired cells/detected photons.

The second part

$$\frac{N_f(N_\gamma)}{N_\gamma}$$

is the ratio between the incident photons and the number of fired cells. For low numbers of incident photons this value equals the PDE and for large number of photons the number of fired cells will aspire to the number of cells of the SiPM and not increase to higher values. That means that for large photon fluxes this part goes against zero.

The third part of the formula

$$\frac{1}{\frac{dN_f(N_\gamma)}{dN_\gamma}}$$

is one over the derivation of the ratio between the number of fired cells and incident photons. For low numbers of incident photons the derivation equals the PDE so that this part and the second part of the formula cancel each other. This part also gives an upper bound of the dynamic range because at the tail of the dynamic range measurement the ratio do not increase any more and the derivation aspires zero and the fraction aspires infinity.

The derivation is calculated like the derivation in the calculation of the breakdown voltage, that means it is a discrete derivation. To calculate the derivation at the discrete point n it is calculated by:

$$\frac{dN_f(n)}{dN_\gamma} = \frac{N_f(n+1) - N_f(n-1)}{N_\gamma(n+1) - N_\gamma(n-1)}.$$

The calculated photon resolution number of both SiPMs is shown in Figure 6.14. It is easy to see that the photon number resolution for the 25 μm SiPM is much smaller and for a bigger range quite linear than the photon number resolution of the 50 μm SiPM.

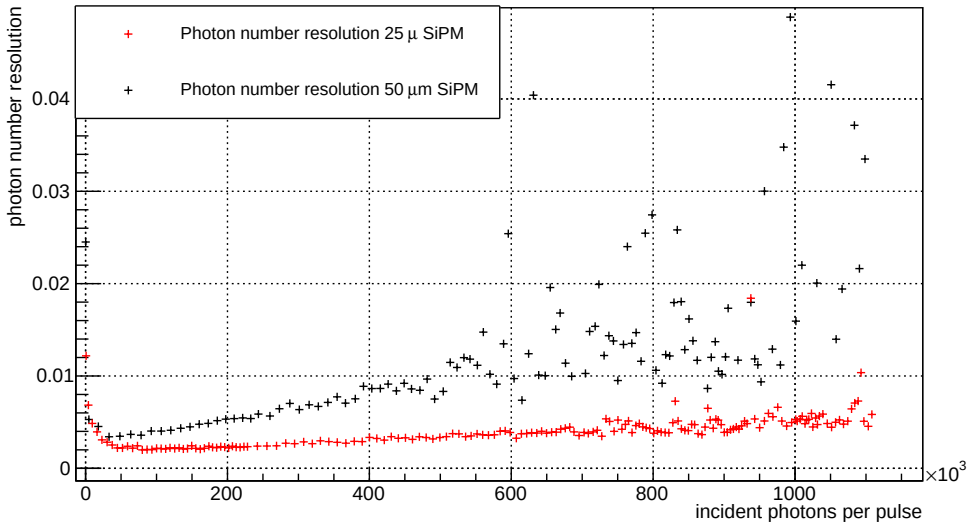

Figure 6.14: Photon number resolution for both SiPM calculated from the data shown in Figure 6.13.

Discussion of the dynamic range measurement

The dynamic range plots are shown in Figure 6.11 and Figure 6.12.

It is easy to see that the detected number of photons is higher than the number of cells of the SiPM. The number of the detected photons is non-saturated for the $25\,\mu m$ SiPM. This could be explained with the large length of the light pulse that were approximated to 250 ns.
Normally a saturation at 1.2 million uniform distributed photons would be expected from simulations [19].
With this pulse length and the Gaussian distribution of the photons it is really hard to give a number of incident photons where the SiPM is saturated.

The $50\,\mu m$ SiPM with 14'400 cells is nearly saturated at nearly 1 million incident photons. Normally a saturation at 180'000 Photons would be expected [19]. This number is 5.5 times higher than the expectation. This is caused by the length of the light pulse and the not uniformed light beam.

This means for the $25\,\mu m$ SiPM that a saturation could be expected at a number of incident photons nearly 6 million. At a small number of photons the measurement coincides with the expectation of a linear slope of the detected photons corresponding to the PDE and the crosstalk probability.

The photon number resolution in Figure 6.14, has a minimum at $\sim 25 \times 10^3$ incident photons for the $50\,\mu m$ SiPM and $\sim 50 \times 10^3$ incident photons for the $25\,\mu m$ SiPM. The small values of the y-axis scale with the error of the number of fired cells. In the simulation it is shown that the simulated values are twice as big [19].
This could be because of a two small estimated or calculated error while the measurement. It is also shown that the photon number resolution of the $25\,\mu m$ SiPM is much smaller and does not increase that rapidly for larger number of incident photons.

A useful dynamic range for the $50\,\mu m$ SiPM could be evaluated up to $\sim 450 \times 10^3$ incident photons for a light pulse of nearly 250 ns. The dynamic range for the $50\,\mu m$ can be evaluated to $\sim 1.6 \times 10^6$ incident photons with the $25\,\mu m$ SiPM. These values are for an one per cent resolution.

Temperature dependency of the dynamic range

The dynamic range of both SiPMs was also measured at a temperature of 10 °C and 35 °C to estimate the temperature dependency. The breakdown voltage was adjusted by the results of the breakdown voltage determination. With this adjusted breakdown voltage the overvoltage and the gain of the measured SiPM has to be constant. This measurement also shows if the results from the breakdown voltage measurement could stabilize the gain.

The dynamic range measurements for the 25 μm SiPM are presented in Figure 6.15. The red curve represents the dynamic range measurement at 35 °C and the blue curve represents the dynamic range measurement at 15 °C.

In Figure 6.16 the dynamic range measurement at 15 °C and 35 °C form the 50μm SiPM is presented.

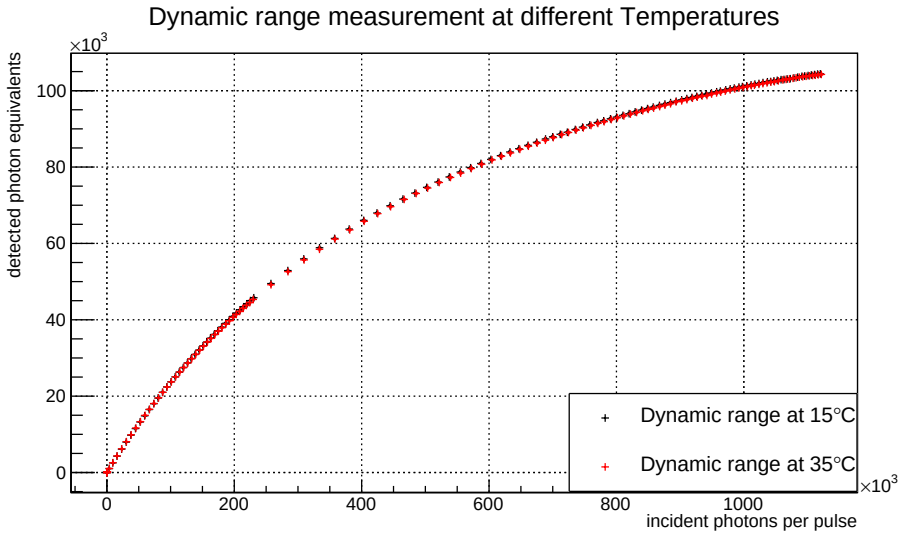

Figure 6.15: Dynamic range measurement at 15 °C and 30 °C for the 25 μm SiPM with an overvoltage of 5 V and a wavelength of $\sim$ 460 nm. Both curves fits over each other which is an indication of a right temperature dependency of the breakdown voltage.

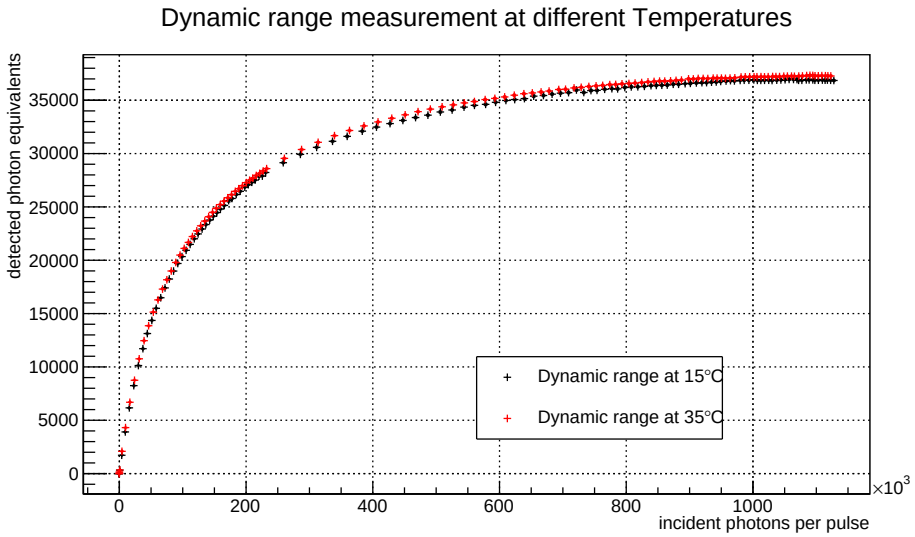

Figure 6.16: Dynamic range measurement at 15 °C and 30 °C for the 50 μm SiPM with an overvoltage of 3 V and a wavelength of $\sim$ 460 nm. The curve do not fit exactly together which shows and inaccurate measured temperature dependency of the breakdown voltage.

For the 25 μm SiPM no temperature dependency of the dynamic range could be seen. For the 50 μm SiPM the curves are not exact equal that shows an temperature dependency. This temperature dependency could be indicative of an inaccurate determined temperature dependency of the breakdown voltage. This inaccurate temperature dependency could cause that the overvoltage is not the same in both measurements. The incorrect overvoltage leads to a different gain that makes the difference in both curves.

Another way to determine the breakdown voltage with special respect to the gain stabilization is presented in the Bachelor-Thesis of C. Güenther: Temperature dependency of the SiPMs and the front-end electronics for Auger Prime [24].

7 Simulation algorithm for the dynamic range

This chapter presents a Monte Carlo simulation programmed with C++ to simulate the dynamic range of the Hamamatsu SiPM. The advantage of this Monte Carlo simulation is, that the beam profile can be fitted to the beam profile of the optical test set-up.

7.1 Simulation algorithm with arbitrary parameters

The simulation uses a simple algorithm to simulate the incident and the detected photons of the SiPM with some arbitrary parameters. The arbitrary parameters are the number of cells N_c of the SiPM, PDE, crosstalk probability ct, length of the light pulse and the recovery time t_r of one cell. Another important parameter is the variance σ^2 of the Gaussian beam profile. This parameter is used if the beam profile over the SiPM equals a Gaussian distribution. The approximation of the beam profile in the chapter about the optical test set-up gives us the beam profile on the SiPM.
The calculations of the algorithm is shown schematically in Figure 7.1.
At first a random number of photons N_γ will be generated. This number of photons will be separated in time packets of 1 ns length. The number of time packets depends on the pulse length. If the number of photons is small against the maximal pulse length the pulse will be calculated with the half of the maximum length. It is possible to separate the photons uniformly or like a Gaussian function.

After this separation a three dimensional array will be created. This array has the following proportions: [number of cells][number of cells][2]. The first two dimensions represent the SiPM where every cell of the array represents a cell of the SiPM. The two cells of the array in the third dimension are for the number of detected photons and the time of the last detected photon. Now the first time step will be simulated. The following steps are done for every time step with the corresponding number of photons in this time steps.
At first a uniform distributed number between zero and one will be diced. If this number is greater then the PDE the photon can not result in an avalanche and the next photon will be tested.
If the number is smaller than the PDE the photon could produce an avalanche.
Now the impact cell of the photon will be simulated. For this two Gaussian distributed numbers are diced. One for the x component and one for the y component of the coordinates of the cell. It is important to say that the mean value of the Gaussian distribution is the cell in the middle of the SiPM. If the x and y coordinate do not lay

inside the range of the SiPM grid the number of incident photons will be decreased by one.
Now the time step of the last entry will be compared with the actual time step. Is it the same time nothing will happen and the next photon will be considered. If it is not the same time packet as the last detected photon it was possible to create an avalanche. To calculate the output, the difference between the incident photon time and the last detection time will be calculated and the high of the detected pulse will be calculated. If it was possible to increase the number of detected photons at this cell another uniform distributed number will be diced. This number will be compared with the crosstalk probability. If it was possible to generate a crosstalk photon the algorithm starts at the point where a possible cell will be calculated.
After doing this for every photon in one time step the next time will be observed. For the next time step the same procedure is done for every photon. After doing this for every time step the number of detected photons will be added and saved. This will be done for different numbers of photons to reproduce the dynamic range.

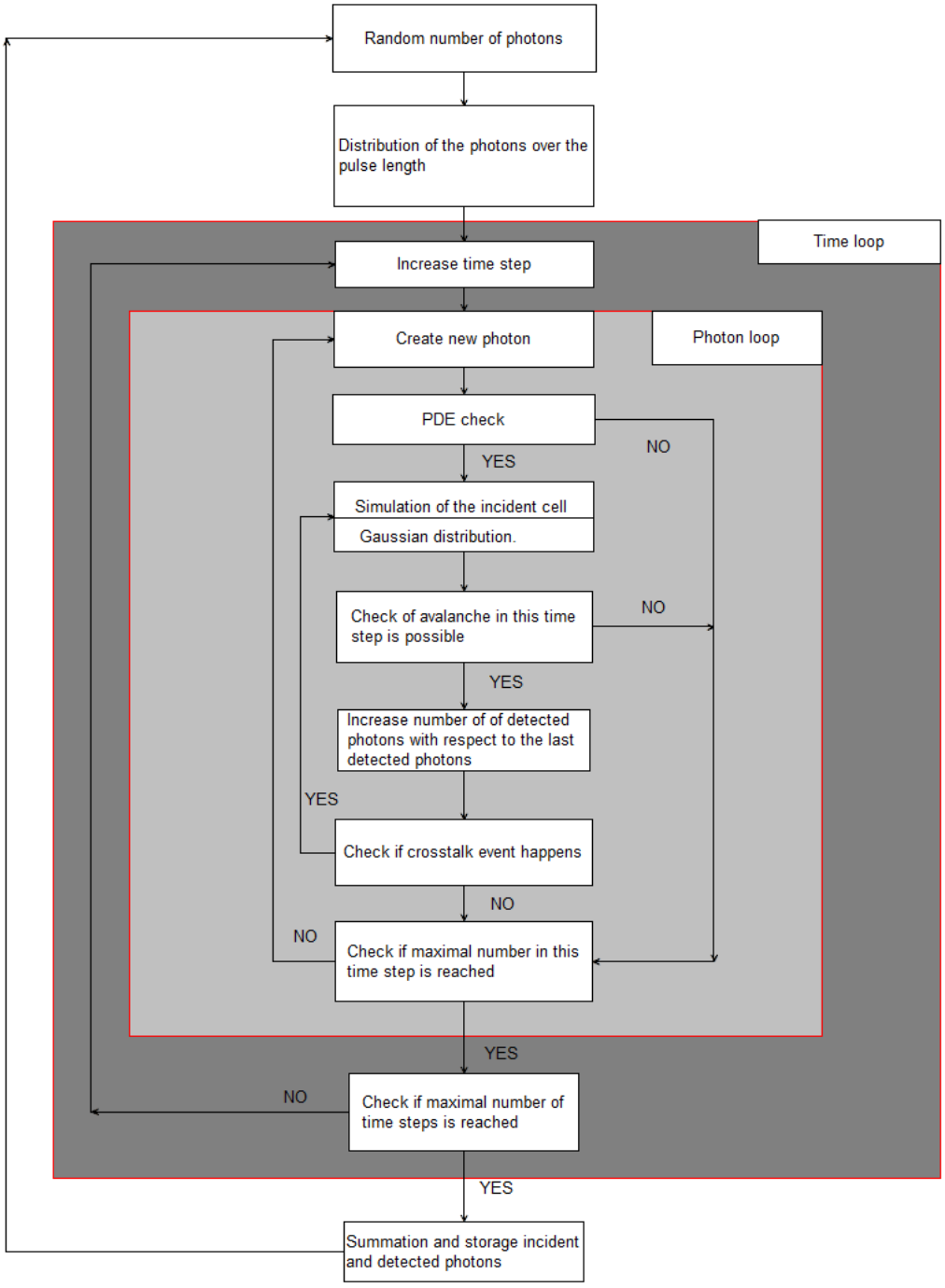

Figure 7.1: Diagram of the simulation algorithm with the two different loops for the calculation of the number of detected photons.

7.2 Results from the simulation

The results from this simple dynamic range simulation are shown in Figure 7.2. The blue curve represents the 25 μm SiPM and the red curve the 50 μm SiPM.
It can be seen that this simple simulation can reproduce the dynamic range measurement with the optical test set up. That the simulation do not fit perfect to the measurement is based on the not perfectly estimated photon flux over the SiPM with the two roughly grids. These two grids are just an approximation of the light flux. Furthermore the positioning of the SiPM is not that exact. Also the light pulse of the simulations conforms not exact the reality. The used light pulse is uniformly but the light pulse from the LED is just in the first approximation uniformly.

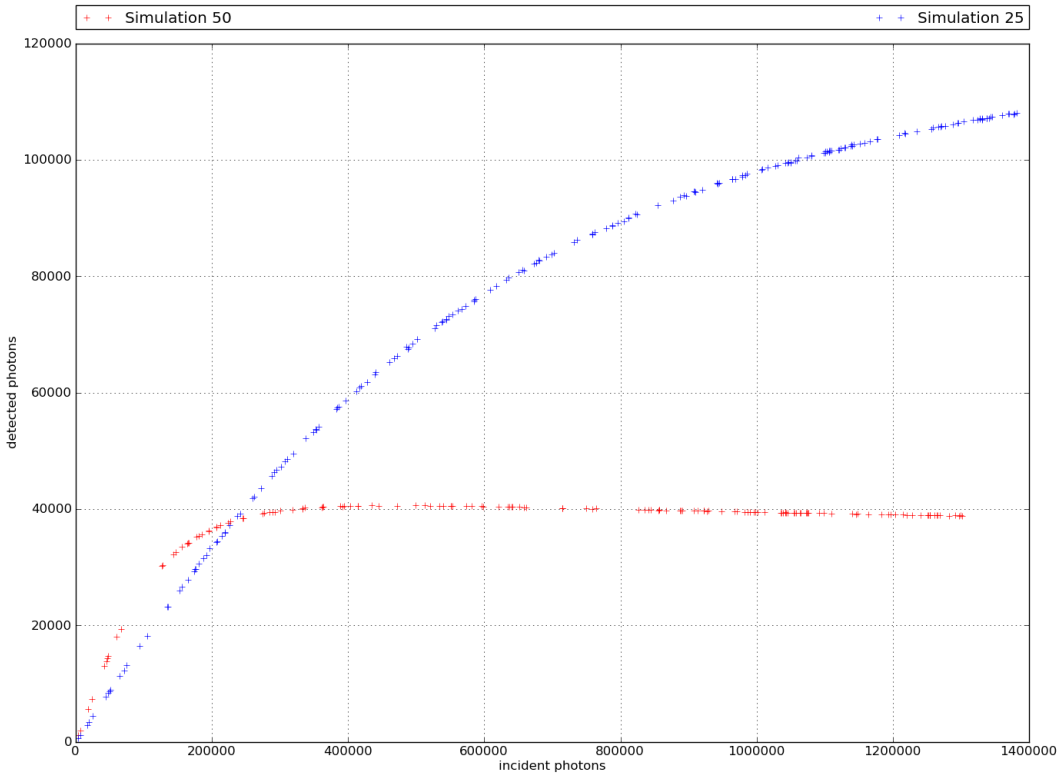

Figure 7.2: Simulated detected photons plotted against simulated incident photons for both SiPMs.

8 Conclusion and outlook

In summary, it can be said, that the dynamic range measurement and determination of the breakdown voltage with the optical test set-up is functional. The measured and estimated results for a useful dynamic range and breakdown voltage with the characteristics that are given by the characteristic of the test set-up are presented in Table 8. Furthermore it could be shown that there is no temperature dependency of the dynamic range if the breakdown voltage was adjusted.

There are some characteristics of the optical test set-up that makes the analyses of the measured data a little bit complicated like the length of the light pulse and not uniform beam profile but it is possible to do a lot of precise measurements to characterise SiPMs.

SiPM	$25\,\mu m$	$50\,\mu m$
$V_{br}\,(25\,°\mathrm{C})\,/\,V$	51.880 ± 0.008	51.7317 ± 0.0016
$\beta\,/\,(mV/K)$	61.52 ± 0.04	60.79 ± 0.05
useful dynamic range / N_γ	$\sim 460 \times 10^3$	$\sim 1.6 \times 10^6$

Table 8: Results from the measurement of the breakdown voltage and the dynamic range with the optical test set up.

To have a better understanding of the dynamic range especially at the range of higher number of incident a dynamic range measurement with a laser could be done. To add some laser diode can give the optical test set-up the opportunity to measure the dynamic range with higher photon fluxes. Furthermore the simulation of the dynamic range has to be adjusted for any form of light fluxes because the light flux on the SiPM has a big impact on the dynamic range of the SiPM.

The determination of the breakdown voltage has to be better understood because there are different methods with different solutions. Also a possible coherence between breakdown voltage and temperature dependency of the SiPM has to be examined.

Bibliography

[1] Cern. Victor Hess discovers cosmic rays. http://timeline.web.cern.ch/victor-hess-discovers-cosmic-rays.

[2] Nobel Media AB 2014. Victor F. Hess - Bibliographical. http://www.nobelprize.org/nobel_prizes/physics/laureates/1936/hess-bio.html.

[3] The Pierre Auger Collaboration. A Detector Thirty Times the size of Paris. https://www.auger.org/index.php/cosmic-rays/detection.

[4] The Pierre Auger Collaboration. The Mystery of High-Energy Cosmic Rays. https://www.auger.org/index.php/cosmic-rays/cosmic-ray-mystery.

[5] Wolfgang Biteneholz. The most powerful particles in the Universe: a cosmic smash. arxiv.org/pdf/1305.1346v1.pdf.

[6] The Pierre Auger Collaboration. The Pierre Auger Observatory I: The Cosmic Ray Energy Spectrum and Related Measurements. https://arxiv.org/ftp/arxiv/papers/1107/1107.4809.pdf, 2011.

[7] The Pierre Auger Collaboration. A Hybrid Detector. https://www.auger.org/index.php/observatory/auger-hybrid-detector.

[8] The Pierre Auger Caloboartion Ruben Conceicao. The Pierre Auger Observatory: results on the highest energy particles. https://arxiv.org/abs/1307.3956.

[9] The Pierre Auger Collaboration. The Pierre Auger Observatory Upgrade "Auger-Prime" Preliminary Design Report. http://arxiv.org/pdf/1604.03637v1.pdf, 2015.

[10] S. Piatek. Physics and operation of an mppc. www.hamamatsu.com/jp/en/community/optical_sensors/physics_of_mppc/index.html, 2014.

[11] AdvanSiD. Introduction to sipms. www.advansid.com/attachment/get/up_89_1411030571.pdf, 09.2014.

[12] HAMAMATSU. Frequently asked questions. www.hamamatsu.com/jp/en/community/optical_sensors/sipm/mppc_faq/inde.html.

[13] First Sensor. Introduction to silicon photomultipliers. http://www.first-sensor.com/cms/upload/appnotes/AN_SiPM_Introduction_E.pdf, 2015.

[14] HAMAMATSU. Mppcs for precision measurement. www.hamamatsu.com/jp/en/community/optical_sensors/sipm/measuring_mppc/index.html, February 2014.

[15] Chen Xu. *Study of the Silicon Photomultipliers and Their Application in Positron Emission Tomography*. PhD thesis, 2014.

[16] S. Piatek. Optical crosstalk in a silicon photomultiplier. www.hamamatsu.com/jp/en/community/optical_sensors/what_is_optical_crosstalk/index.html, feb 2016.

[17] HAMAMATSU. Measuring the electrical and optical properties of an mppc. www.hamatsu.com/resources/pdf/ssd/s13360_series_kapd1052e.pdfs, May, 2016.

[18] SensL. An Introduction to the Silicon Photomultipliers. www.sensl.com/downloads/ds/TN-IntrotoSPMTech.pdf, oct 2011.

[19] Thomas Bretz. SiPM-4-SSD, Jun 2015.

[20] Carsten Heidemann. Optical Set-Up for Automised SiPM Characterisation. Will be published in 2016, 2016.

[21] SensL. C-Series Datasheet. www.sensl.com/downloads/ds/DS-MicroCseries.pdf, 2014.

[22] AdvanSiD. NUV SiPMs Chip Scale Package. advansid.com/attachment/get/up_53_1432731710.pdf, 2015.

[23] Excelitas. C30742-66 Series Datasheet. www.excelitas.com/downloads/dts_c30742-66_series_sipm.pdf, 2010.

[24] Christop Günther. Temperature dependency of the SiPMs and the front-end electronics for Auger Prime. Will be published in 2016, 2016.

Acknowledgments

Ich bedanke mich bei Herrn Prof. Bretz und Herrn Prof. Hebbeker, dass mir die Möglichkeit gegeben wurde, an diesem Institut meine Bachelorarbeit anzufertigen. Des Weiteren gilt großer Dank Johannes Schumacher für seine Unterstützung beim Anfertigen dieser Arbeit, sei es bei verschiedenen Fragen bezüglich des Themas oder bei der Korrektur dieser Arbeit. Er hat mit seinen immer neuen Verbesserungsvorschlägen zum Gelingen dieser Arbeit beigesteuert. Auch möchte ich Carsten Heidemann sehr danken, zunächst einmal dass ich mit seinem Aufbau messen durfte und dass er mir alle Fragen zum Messaufbau stets schnell beantwortet hat. Ein Dank gilt auch der Elektronikwerkstatt für das Herstellen der zum Messen notwendigen Platine. Auch möchte ich mich bei meinen Büro- und Flurnachbarn und Institutskollegen für die schöne Zeit am Institut bedanken, welche auch immer auf meine Fragen die passende Antwort wussten.
Dann danke ich zu guter Letzt auch meiner Familie und meinen Freunden, welche während der Anfertigung dieser Arbeit ziemlich viel auf mich verzichten mussten, aber ohne deren Unterstützung diese Arbeit nicht möglich gewesen wäre.

Eidesstattliche Versicherung

Ich versichere hiermit an Eides Statt, dass ich die vorligende Bachelorarbeit mit dem Titel "Measurement of the dynamic range of SiPMs for Auger Prime" selbstständig und ohne unzulässige fremde Hilfe erbracht habe. Ich habe keine anderen als die angegebenen Quellen und Hilfsmittel benutzt. Die Arbeit hat in gleicher oder ähnlicher Form noch keiner Prüfungsbehörde vorgelegen.

Aachen, den 31.07.2016

(Alexander Gutsche)